AGU PUBLICATIONS

Geochemistry, Geophysics, Geosystems

RESEARCH ARTICLE
10.1002/2014GC005484

Companion to *Kaban et al.* [2014], doi:10.1002/2014GC005483

Key Points:
- A new inversion technique using gravity and seismic tomography data is applied
- Improved thermal and density models of the upper mantle are developed
- In the cratons, density varies more significantly than temperature

Correspondence to:
M. Tesauro,
M.Tesauro@uu.nl

Citation:
Tesauro, M., M. K. Kaban, W. D. Mooney, and S. A. P. L. Cloetingh (2014), Density, temperature, and composition of the North American lithosphere—New insights from a joint analysis of seismic, gravity, and mineral physics data: 2. Thermal and compositional model of the upper mantle, *Geochem. Geophys. Geosyst.*, *15*, 4808–4830, doi:10.1002/2014GC005484.

Received 16 JUL 2014
Accepted 16 NOV 2014
Accepted article online 20 NOV 2014
Published online 10 DEC 2014

Density, temperature, and composition of the North American lithosphere—New insights from a joint analysis of seismic, gravity, and mineral physics data: 2. Thermal and compositional model of the upper mantle

Magdala Tesauro[1,2], Mikhail K. Kaban[1,3], Walter D. Mooney[4], and Sierd A. P. L. Cloetingh[2,5]

[1]GeoForschungsZentrum Potsdam, Potsdam, Germany, [2]Department of Earth Sciences, Utrecht University, Utrecht, Netherlands, [3]Geophysical Center, IPE, RAS, Moscow, Russia, [4]U.S. Geological Survey, Menlo Park, California, USA, [5]Ludwig-Maximilians University of Munich, Earth and Environmental Sciences, Munich, Germany

Abstract Temperature and compositional variations of the North American (NA) lithospheric mantle are estimated using a new inversion technique introduced in Part 1, which allows us to jointly interpret seismic tomography and gravity data, taking into account depletion of the lithospheric mantle beneath the cratonic regions. The technique is tested using two tomography models (NA07 and SL2013sv) and different lithospheric density models. The first density model (Model I) reproduces the typical compositionally stratified lithospheric mantle, which is consistent with xenolith samples from the central Slave craton, while the second one (Model II) is based on the direct inversion of the residual gravity and residual topography. The results obtained, both in terms of temperature and composition, are more strongly influenced by the input models derived from seismic tomography, rather than by the choice of lithospheric density Model I versus Model II. The final temperatures estimated in the Archean lithospheric root are up to 150°C higher than in the initial thermal models obtained using a laterally and vertically uniform "fertile" compositional model and are in agreement with temperatures derived from xenolith data. Therefore, the effect of the compositional variations cannot be neglected when temperatures of the cratonic lithospheric mantle are estimated. Strong negative compositional density anomalies (<-0.03 g/cm^3), corresponding to Mg # ($100 \times$ Mg/(Mg + Fe)) >92, characterize the lithospheric mantle of the northwestern part of the Superior craton and the central part of the Slave and Churchill craton, according to both tomographic models. The largest discrepancies between the results based on different tomography models are observed in the Proterozoic regions, such as the Trans Hudson Orogen (THO), Rocky Mountains, and Colorado Plateau, which appear weakly depleted (>-0.025 g/cm^3 corresponding to Mg # $\sim$91) when model NA07 is used, or locally characterized by high-density bodies when model SL2013sv is used. The former results are in agreement with those based on the interpretation of xenolith data. The high-density bodies might be interpreted as fragments of subducted slabs or of the advection of the lithospheric mantle induced from the eastward-directed flat slab subduction. The selection of a seismic tomography model plays a significant role when estimating lithospheric density, temperature, and compositional heterogeneity. The consideration of the results of more than one model gives a more complete picture of the possible compositional variations within the NA lithospheric mantle.

1. Introduction

Density heterogeneity in the upper mantle, which is responsible for the dynamics of the continents, originates from temperature and compositional variations. Therefore, the separation of the two effects is fundamental for understanding the evolution of our planet. Previous geophysical studies aimed to estimate both temperature and compositional variations on a global [e.g., *Deschamps et al.*, 2002; *Simmons et al.*, 2009] and regional scale [e.g., *Godey et al.*, 2004; *Khan et al.*, 2011, 2013] in the upper mantle, linking seismic velocity to density perturbations through relative scaling of the conversion factor ($R\rho/s = \mathrm{d}\ln\rho/\mathrm{d}\ln V_s$) or applying a probabilistic approach, aiming to invert seismological data directly into the thermochemical structure [*Khan et al.*, 2011, 2013]. However, these techniques consider variations of only one parameter (seismic velocity or phase-velocity maps) to estimate several others. Therefore, an infinite number of solutions can be obtained, besides the preferred one. In Part 1 [*Kaban et al.*, 2014], we have presented a newly developed

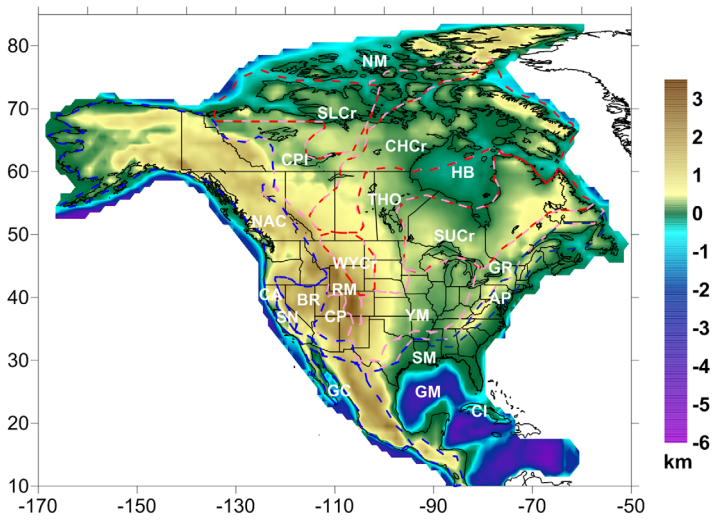

Figure 1. Topographic map of North America, taken from ETOPO2 [*NOAA*, 2010]. Red, pink, and blue dashed contours show the boundaries between the Archean, Proterozoic and Phanerozoic geological provinces, delineated taking into account the crustal age, the geographical extension of the key tectonic elements and the physiographical boundaries [modified after *Tesauro et al*., 2014]. White labels stand as follows: AP, Appalachians; BR, Basin and Range; CA, Cascadia; CHCr, Churchill craton; CI, Cuba Island; CP, Colorado Plateau; CPl, Canadian Platform; GC, Gulf of California; GM, Gulf of Mexico; GR, Grenville; HB, Hudson Basin; NAC, North American Cordillera; NM, North Margin; RM, Rocky Mountains; SLCr, Slave craton; SM, South Margin; SN, Sierra Nevada; SUCr, Superior craton; THO, Trans-Hudson Orogen; WYCr, Wyoming craton; YM, Yavapai-Maztzal.

inversion technique that jointly utilizes gravity and seismic tomography data to simultaneously estimate thermal and compositional density heterogeneity in the upper mantle. To test this technique, we chose as a study area the North American (NA) continent (10°N by 85°N and 170°W by 50°W), which is composed of a mosaic of tectonic provinces of different age (Figure 1). Archean cratons are located in the central and eastern part of North America, including the Slave, Churchill (Rae and Hearne), Superior, and Wyoming cratons. These cratonic blocks were assembled during the Proterozoic, accompanied by the accretion of additional, smaller terrains. Formation of orogenic belts occurred during the Phanerozoic, most notably with the accretion of the Appalachian belt on the east coast [e.g., *Thomas*, 1989] during the Paleozoic and of the Western Cordillera [e.g., *Dickinson*, 2004] during Mesozoic-Cenozoic time.

In *Kaban et al*. [2014], we first computed mantle gravity anomalies and residual topography by estimating the gravity effect of the crust. The latter was evaluated using as input NACr14, the most recent NA crustal model, providing thickness and average velocity of the three layers that comprise the crystalline crust [*Tesauro et al*., 2014]. The joint inversion of the residual mantle gravity anomalies and the residual topography allowed the construction of a preliminary 3-D density model, reflecting the effect of both thermal and compositional variations in the upper mantle. Successively, we inverted for temperature of the upper mantle the regional NA07 [*Bedle and van der Lee*, 2009] and the global SL2013sv [*Schaeffer and Lebedev*, 2013] tomography models, based on similar data and assumptions in order to evaluate possible discrepancies due to using different tomography data. In fact, as discussed before [*Kaban et al*., 2014], the amplitudes of the seismic anomalies may differ significantly for various seismic tomographic models depending on the method used. In the inversion for mantle density, we used a uniform composition representative of a "fertile" mantle, affected by a small amount of melt extraction. This composition (Table 1) was defined as an average of the mineral fractions constituting the "Primitive mantle" rock [*McDonough and Sun*, 1995] and the "Tecton garnet peridotite" rock [*Griffin et al*., 2003]. These initial thermal models were used to separate the effect of temperature and composition in the mantle residual gravity anomalies, estimated by subtracting the gravity effect of the crust from the observed gravity field. These preliminary results permit the identification of those parts of the cratons characterized by an anomalous low-density upper mantle and the possible presence of high-density bodies in the Proterozoic craton and in the Phanerozoic off-craton regions. However, the vertical and lateral uniform "fertile" composition used to estimate the temperature

Table 1. Mineral Fractions and Mg # (100 × Mg/(Mg + Fe)) for the Two End-Members Compositions Used in This Study[a]

	Olivine (%)	OPX (%)	CPX (%)	Garnet (%)	Mg #
Primitive mantle	58.5	15	11.5	15	89
Depleted mantle	69.5	21	4	5.5	94

[a]See text for further explanation.

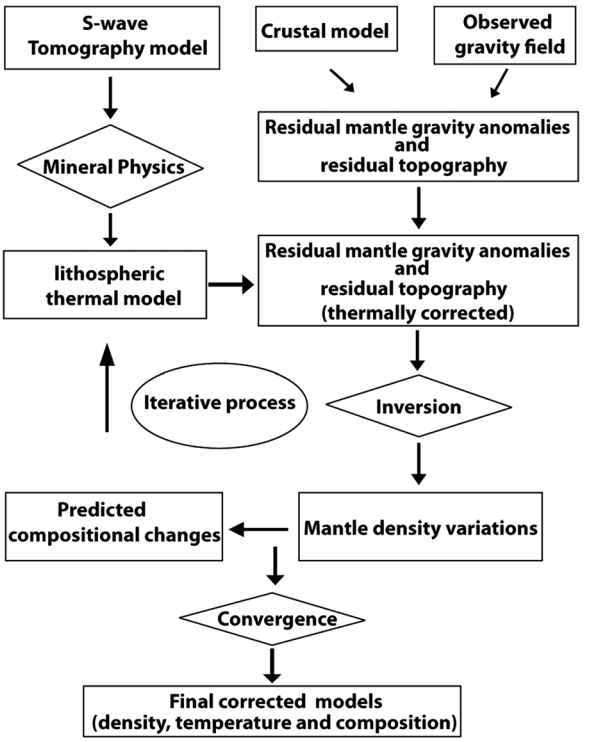

Figure 2. Workflow showing the main steps of the iterative technique applied in this study. See text for further explanation.

variations was representative of the mineralogy of Phanerozoic, rather than Precambrian, upper mantle. Therefore, not considering compositional variations, might result in large errors in the temperatures estimated for the cratons [e.g., *Goes et al*., 2000], which are usually characterized by a lithospheric mantle depleted in high-density constituents (e.g., garnet (Gt) and Fe).

In this study, we apply the iterative technique presented in the study of *Kaban et al*., [2014] to correct the initial thermal fields for the compositional effect in the cratonic regions. Our aim is to obtain a more realistic model for the lithospheric mantle thermal and compositional structure. We first evaluate, using mineral physics equations [*Stixrude and Lithgow-Bertelloni*, 2005], the effect that variations of the proportion of the main minerals and high-density components (Fe) of the lithospheric mantle have on its density and seismic velocity (Appendix A). Successively, we estimate the compositional changes occurring in the cratonic lithospheric mantle, with respect to a "fertile" mantle composition, in terms of Mg # (the molar ratio100 $\times$ Mg/(Mg + Fe)) and percentage of mineral fractions. The new composition is estimated by compensating the initial residual ("compositional") densities, evaluated in *Kaban et al*. [2014], with the density of a rock having a different Mg # and percentage of mineral fractions, with respect to the "fertile" peridotite. In this way, we estimate again the temperatures, according to the new composition, and repeat the previous steps described until convergence is reached (Figure 2). Therefore, the final results provide estimates of the thermal and compositional state of the NA lithospheric mantle that are consistent with all data. Since we do not have tight constraints on the lateral thickness variations of the NA lithosphere, we extend our model up to a depth of 300 km, which includes the entire lithosphere and a small part of the sublithospheric mantle.

2. Compositional Variations in the Lithospheric Mantle Under the Craton

Previous studies based on interpretations of xenolith data [e.g., *Lee*, 2003; *Griffin et al*., 2003, 2004; *Kopylova et al*., 2004; *Carlson et al*., 2004; *Matsukage et al*., 2005] have revealed how compositional heterogeneity influences the density and seismic velocity of the upper mantle. The Archean subcontinental lithospheric mantle (SCLM) is generally characterized in its uppermost part (at a depth of 100 km and temperature of $\sim$700°C) by high *P* and *S* wave velocities ($\sim$8.20 and $\sim$4.70 km/s, respectively) and a significantly lower density ($\sim$3.31 g/cm^3) compared to Proterozoic (8.10 km/s, 4.60 km/s, and 3.34 g/cm^3, respectively) and to Phanerozoic (7.90 km/s, 4.50 km/s, and $\sim$3.37 g/cm^3, respectively) SCLM [e.g., *Griffin et al*., 2003]. Such a seismic and density signature characterizing the lithospheric mantle of the Archean and Proterozoic cratons is related to its chemical differentiation that occurred during melt extraction [e.g., *O'Hara et al*., 1975]. The Archean lithospheric mantle is commonly strongly stratified with regard to chemical composition and lithology, and contains rock types depleted in high-density components, which are essentially absent in the Phanerozoic SCLM. Variations in composition related to age of the continental lithosphere are well known [e.g., *Hawkesworth et al*., 1990; *Gaul et al*., 2000; *Poudjom Djomani et al*., 2001]. *Jordan* [1979] was the first to recognize the importance of the effect of chemical differentiation on seismic wave velocities and density based

on his analysis of the variation of these parameters from a suite of ultramafic rocks from southern Africa. Subsequent studies [e.g., *Griffin et al*., 2003, 2004; *Carlson et al*., 2004; *Lee*, 2003; *Lee et al*., 2011; *Kopylova et al*., 2004; *Matsukage et al*., 2005] investigated the same variations in the Gt and spinel (Sp) peridotites, typically sampled by deep seated magmas, such as alkaline basalts and kimberlites. Peridotite is the most abundant mantle rock type and also the dominant rock recovered as xenolith [e.g., *Pearson et al*., 2003], with eclogite, the high-pressure equivalent of basalt, of secondary abundance. However, the overall abundance of eclogite in the cratonic root appears to be 1% or less, although may locally reach 3–15%, according to xenolith data [*Schulze*, 1989].

The compositional heterogeneity of peridotites in the lithospheric mantle is represented by different volume fractions of its three main constituents: olivine (Ol), pyroxenes, and an aluminous phase (mostly Sp or Gt at a depth higher than 50–60 km). Peridotites, which have experienced minor amounts of melt extraction, are characterized by Mg # of ~86–89 and significant amounts (usually >10%) of clinopyroxene (CPX), orthopyroxene (OPX) and Gt in addition to Ol (>50%) [e.g., *Lee*, 2003]. When such peridotites, classified as lherzolites, start to melt, CPX and Gt are preferentially extracted by the melt relative to Ol and OPX, with increasing temperature or decreasing pressure [e.g., *Walter*, 2003]. With increasing degree of melt extraction, residual CPX decreases to <5 wt % and peridotites classified as harzburgites are generated [*Streckeisen*, 1976]. When enough melt has been extracted (e.g., >30 wt %) to exhaust not only the CPX but also the OPX (<10 wt %), an Ol-rich residue (dunite) is formed [e.g., *Lee*, 2003; *Walter*, 2003]. At the same time, the residual rocks are depleted in some major elements (e.g., SiO_2, Fe, Al_2O_3, CaO) with respect to some others (e.g., MgO), depending on the pressure of melt extraction [*Walter*, 2003]. The high Mg/Si ratio and Mg # of many of the Archean peridotites compared with those of Phanerozoic peridotites require higher degrees of melt extraction [e.g., *Griffin et al*., 2003]. Therefore, the Mg # of bulk rock (and silicate minerals), which increases with an increase in degree of partial melting and melting extraction, is a good indicator of depletion. The Ol content usually increases from a lherzolite to a harzburgite from 55 to 85 vol % [*Matsukage et al*., 2005]. Therefore, in general, the concentration of compatible elements increases and of incompatible elements decreases with increasing modal proportion of Ol. However, the Ol fraction in some continental peridotites does not show a clear correlation with Mg #, because of an excess of OPX [e.g., *Boyd*, 1989; *Lee*, 2003; *Matsukage et al*., 2005]. For instance, some peridotites, such as found in the Kaapvaal and Siberian cratons [e.g., *Boyd et al*., 1997], with high Mg # (>92) contain an extremely large amount of OPX (up to 45 vol %). The excess in OPX in these samples, characterized by higher Si/Mg, is probably the result of additional petrogenetic processes (e.g., the infiltration of silicic melts or fluids), superimposed on earlier melt extraction events [*Boyd*, 1989; *Griffin et al*., 2003; *Carlson et al*., 2004; *Lee and Chin*, 2014]. Refertilization of the lithospheric mantle, may also cause further changes in the mineral modes, such as the addition of Ol by a silica undersaturated melt [*Kelemen et al*., 1998] and of CPX and Gt by basaltic melts [e.g., *Boyd et al*., 1997]. Therefore, refertilization may have an effect on composition and mineralogy which mimics a lower degree of melt extraction in initially strongly depleted Archean lithospheric mantle [e.g., *Griffin et al*., 2003].

3. Assumptions on Lithospheric Mantle Composition of the NA Continent

The mean composition of peridotites of the NA cratons is progressively less depleted in incompatible elements from Archean, through Proterozoic to Phanerozoic time, reflecting a secular decrease in the average degree of melt extraction from newly created lithospheric mantle [e.g., *Griffin et al*., 2003]. Indeed, most of the Proterozoic SCLM contains a high proportion of fertile xenoliths, which may represent metasomatic refertilization of previously depleted rocks [*Griffin et al*., 2009; *Lee et al*., 2011]. Despite the large scatter in Mg # in the xenoliths of the NA cratons, a general positive correlation of Mg # with the Ol and OPX fractions and an inverse correlation with the CPX and Gt fractions are found [e.g., *Griffin et al*., 2004].

On the basis of the above considerations, we assume that the lithospheric mantle composition beneath the NA cratons changes in a range given by a linear variation of mineral fractions ("lithological changes") and Mg # ("chemical changes") between two end-member compositions (Table 1). This assumption for the mineral fractions is valid at least for Ol [*Walter*, 1998].

The first composition ("fertile" composition) is used to estimate the initial thermal model and, as before discussed, is more representative of the little depleted Phanerozoic lithospheric mantle. The second end-member composition represents a strongly depleted lithospheric mantle ("refractory" composition) (Table 1),

on account of the large melt extraction. It is composed by an average of the mineral fractions constituting the "Archon" and "Proton" composition defined by *Griffin et al*. [2003], as the most representative rocks of the Archean and Proterozoic NA SCLM. We associate to this lithospheric mantle composition a Mg # 94, which is the highest common value for very depleted peridotites [e.g., *Griffin et al*., 2003]. On account of the wide scatter of Mg # in the continental peridotites [e.g., *Lee*, 2003], the mineral fractions composing the rocks might diverge from those assumed here for a specific Mg #. In addition, variations of mineral fractions and Mg # may occur by varying pressure (*P*) and temperature (*T*) conditions [e.g., *Griffin et al*., 2009; *Matsukage et al*., 2005]. On the other hand, these changes are generally very small in the range of physical conditions of the mantle lithosphere. Therefore, with the two end-members compositions we intend to represent generally the less depleted and strong depleted lithospheric upper mantle of the NA continent, without considering local possible deviations.

Furthermore, we should emphasize that we are assuming that the lithospheric mantle compositional variations of the NA cratons are only related to the degree of depletion, in terms of Mg # and of the mineral fractions considered. In fact, other minerals may contribute to decrease the density of the lithospheric mantle, like Sp, which is usually present in place of Gt in the uppermost mantle ($<$100 km) [e.g., *Griffin et al*., 2004]. This mineral might be more abundant in the lithospheric mantle underlying the cratons, due to chromium (Cr) addition. In fact, the latter would not only shift the phase transition of Sp-Gt to higher pressures (from 3 up to 7 GPa) but also make it spread over a broad depth interval [*Klemme*, 2004]. We do not include the Sp phase in our model in the absence of sufficient constraints on the amount of Cr present in the NA lithospheric mantle. Seismic velocity and density variations might also depend on other local compositional effects not considered here, such as an unusual high proportion of eclogite or metasomatic eclogite, as in a part of the Slave craton [e.g., *Kopylova et al*., 2004].

4. Application of the Iterative Technique

Previous interpretations of NA xenoliths of Archean and Proterozoic age have often demonstrated a progressive decrease of depletion with depth [e.g., *Gaul et al*., 2000; *Griffin et al*., 2003]. In other cases, as for the central part of the old ($\geq$2.7 Gy) Slave craton, the lithospheric mantle shows two zones, a shallow ultradepleted layer (between 100 and 150 km) dominated by Gt harzburgite and a deeper more fertile layer, strongly dominated by Gt lherzolite [e.g., *Menzies et al*., 2004; *Griffin et al*., 1999, 2004]. Since, as previously discussed, a more depleted composition has a strong influence on the density and velocity of the lithospheric mantle, we use the iterative approach (Figure 2), discussed in the study of *Kaban et al*. [2014] to correct the initial thermal fields for compositional variations due to depletion.

We have initially estimated the mantle gravity anomalies by subtracting the gravity effect of the crust (NACr14) [*Tesauro et al*., 2014] from the observed gravity field. Successively, we have evaluated the thermal component of the gravity anomalies using the initial thermal models and subtracted it from the total mantle anomalies, in order to obtain the residual field, which should reflect compositional heterogeneity not taking into account uncertainties in the temperature estimation [*Kaban et al*., 2014]. Then, we assume that the decrease of the upper mantle densities in the cratonic regions is related to compositional heterogeneity not considered in the first inversion of the tomographic models. Therefore, we fit the density decrease by different degree of depletion in high-density constituents, in respect to the initial "fertile" peridotite. We estimate the temperatures according to the new composition and the anelasticity model Q3 [*Cammarano et al*., 2003], more representative for the generally "dry" conditions characterizing the cratonic lithospheric mantle. Local deviations from the "dry" conditions might be expected in the refertilized part of the craton. They may cause an overestimation of temperatures of $\sim$100°C [*Cammarano et al*., 2003], corresponding to a gravity effect of $<$100 mGal [*Kaban et al*., 2014, Part 1], when the anelasticity starts to be activated at a temperature of $\sim$900°C [*Jackson et al*., 2002]. The newly estimated gravity anomalies induced by temperatures are again subtracted from the total mantle gravity field in order to obtain the residual field and convert it to density variations. This iterative process is repeated until the convergence is reached.

The negative density variations are distributed with depth according to two different models. With the first model (Model I), we aimed to reproduce the typical change of composition of the lithospheric mantle with depth, which is observed in xenolith samples of the central Slave craton. We assume up to a depth of 150 km a maximal (constant) degree of depletion, while below a linear decrease of it up to a depth of

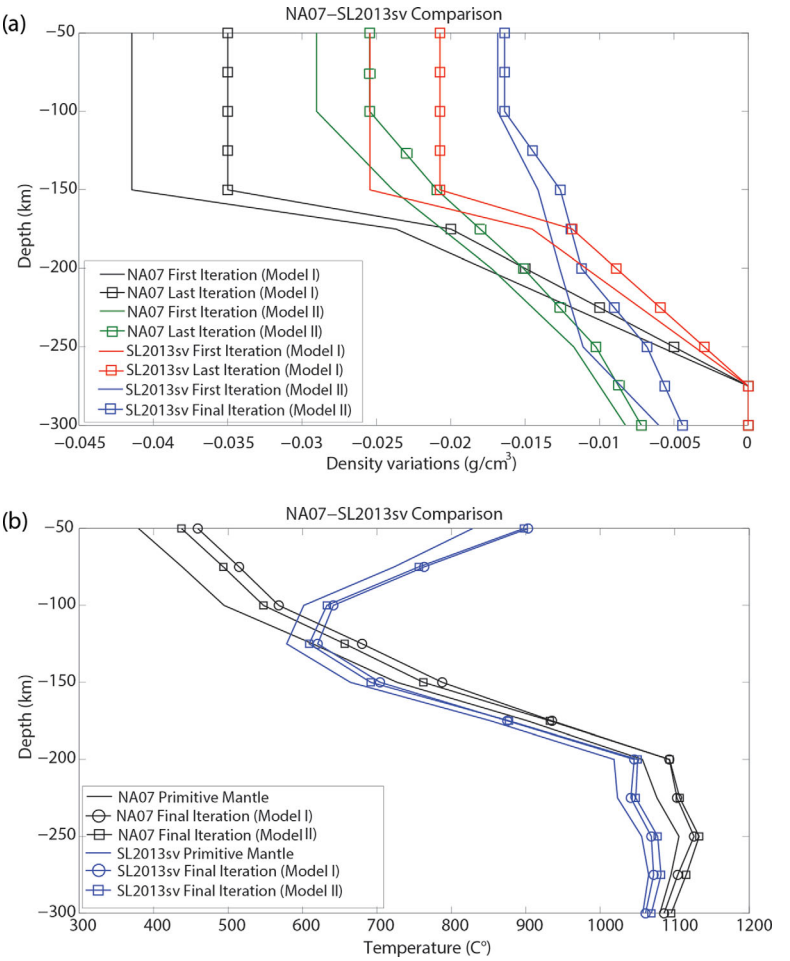

Figure 3. (a) Average residual ("compositional") density variations, in a representative part of the cratons (see Figures A1a–A1d), vertically distributed according to two models (Model I reproducing the typical compositionally stratified lithospheric mantle and Model II based on the direct inversion of the residual gravity and residual topography) and two seismic tomography models, NA07 [*Bedle and van der Lee*, 2009] and SL2013sv [*Schaeffer and Lebedev*, 2013]; (b) average temperatures estimated in the first and last iteration from the inversion of the indicated tomographic model, using a mantle composition, whose density compensates the average residual density variations displayed in the top plot (Figure 3a). See text for further explanation.

275 km, where the composition becomes equal to that of the "fertile" composition. Such a compositional layering has before been argued to explain changes in the direction of azimuthal anisotropy with depth under the NA Archean core [*Yuan and Romanowicz*, 2010] and to satisfy other geophysical and petrological observations (e.g., geoid, surface heat flow, and seismic velocities) of the cratons [*Afonso et al*., 2008]. The second model of density distribution (Model II) is based on the direct inversion of the residual gravity and residual topography [*Kaban et al*., 2014; M. K. Kaban et al., Cratonic roots under North America are shifted by basal drag: New evidence from gravity and geodynamic modeling, submitted to *Nature Geoscience*, 2014]. This distribution, being almost linear below the depth of 100 km, might be more representative of other parts of the cratonic lithospheric mantle, which are not characterized by an ultradepleted shallow lithospheric mantle [e.g., *Griffin et al*., 2004]. The residual density variations in the uppermost mantle are less in amplitude than in Model I likely because of damping applied in the inversion to stabilize the solution (Kaban et al., submitted manuscript, 2014). The uncertainty of the density variations obtained in the inversion depends more strongly on the assumed distribution of the density with depth (based on the assumed seismic tomography model) than on the gravity inversion. Speaking about the effect of the uncertainty of the residual gravity field, which is translated into density perturbations, an error of 100 mGal corresponds to the density uncertainty of about 0.005 g/cm^3 attributed to a layer thick 200 km. Since most of the anomalies are concentrated within the upper 100 km, this value can be increased by about 50%, which yields a density uncertainty of about 0.0075 g/cm^3.

Assuming a linear variation between the two end-members defined in section 3, the minimum value of depletion is represented by a change in the corresponding fractions of the main mineral constituents (Ol: +0.22%, OPX: +0.12%, CPX: −0.15% Gt: −0.19%) and by a 0.1 increase in the Mg # of the bulk rock. The mineral phases are treated as an ideal solid solution of Mg and Fe species (end-members) and, in case of Gt, also of Ca species (end-member): Ol (forsterite + fayalite), OPX (enstatite), CPX (diopside + hedenbergite), Gt (pyrope + almandine + glossular). Therefore, variations of Mg # imply variations of the percentage of Fe and Mg species, while the amount of Ca end-member of the Gt (glossular) is taken as constant (20%). The minimum amount of depletion compensates a density variation of −0.0016 g/cm^3. Such a value was estimated on the basis of the tests performed to evaluate the influence of Mg # and variations in the mineral fractions on density (Appendix A). Density variations lower than this value or positive values are not compensated and the initial "fertile" composition remains unchanged. We are aware that the density variations can be compensated by compositions different by those defined, but with our assumptions we try to represent realistically the depletion of the cratonic lithospheric mantle. Thus, our goal in this study is to obtain a petrologically realistic interpretation of the density variations in the cratonic lithospheric mantle. This goal is more difficult to achieve solely from the analysis of xenoliths, on account of their uneven distribution, large scatter in composition and their generally shallow depth of formation (relatively few of them originate at a depth ≥200 km) [e.g., *Lee*, 2003; *Griffin et al*., 2003, 2004]. In the off-craton regions, we did not apply this iteration process, but instead we use the initial uniform composition ("fertile") and the anelasticity model Q4 [*Cammarano et al*., 2003], which is more suitable for the wet lithospheric mantle characterizing these areas. Therefore, in this case, we interpret the residual density variations obtained as depending on compositional changes different from depletion.

We estimate the average residual density variations in a selected part of the NA cratons and present the results after the first and last iteration (Figure 3a), using Model I and Model II to distribute the residual density variations with depth and the two seismic tomography models, NA07 [*Bedle and van der Lee*, 2009] and SL2013sv [*Schaeffer and Lebedev*, 2013]. The models of density variations, which are discussed here and in the next sections, are identified with the same names of the two seismic tomography models. We notice that the values of the residual density variations estimated for model NA07 are ∼0.015 g/cm^3 larger than those estimated for model SL2013sv. In addition, the residual density variations for model NA07 are larger in the shallowest upper mantle compared with results from model SL2013sv, while the opposite occurs below 200 km. At a depth close to the lower boundary of the lithosphere (≥250 km), the average residual density decreases to values lower than 0.01 g/cm^3, which implies an almost "fertile" composition. The largest difference in the average residual density variations between the first and the last iteration occurs in the uppermost mantle, when the first depth distribution is assumed, and is equal to ∼0.007 g/cm^3 and ∼0.0025 g/cm^3 in NA07 and SL2013sv, respectively. Such a difference, according to Model II decreases to ∼0.0025 g/cm^3 in NA07 and becomes even smaller in SL2013sv.

For the same area and two seismic tomography models, we have also estimated the average temperature, using the composition corresponding to the first and last iteration (Figure 3b). We note that below 100 km the inversion of the two tomographic models results in ∼50°C higher temperatures for NA07 compared to SL2013sv, while above this depth model SL2013sv shows up to ∼400°C higher temperatures than model NA07. Such a strong difference, due to the relatively low (and likely unrealistic) velocities estimated in SL2013sv at shallow depths, causes in the same model a negative temperature gradient in the depleted lithospheric mantle. We note that, for both models, the difference in temperatures between the first and last iteration at 100 km is not large (∼100°C) and is generally less than 50°C below the depth of 250 km. In addition, the temperatures obtained after the last iteration, using Model I and Model II and the same tomographic model, are very similar.

5. Final Thermal Model

As described in Part 1 [*Kaban et al*., 2014], we estimate the temperatures during the iterative process by inverting both the NA07 and SL2013sv seismic tomography models (Figures 4a–4d), applying the mineral physics approach of *Stixrude and Lithgow-Bertelloni* [2005]. We use the elastic modulus and their pressure derivative of the mineral phases defined in *Cammarano et al*. [2003], which are estimated taking into account their dependence on the iron content. All other properties of the mantle, taken from *Stixrude and*

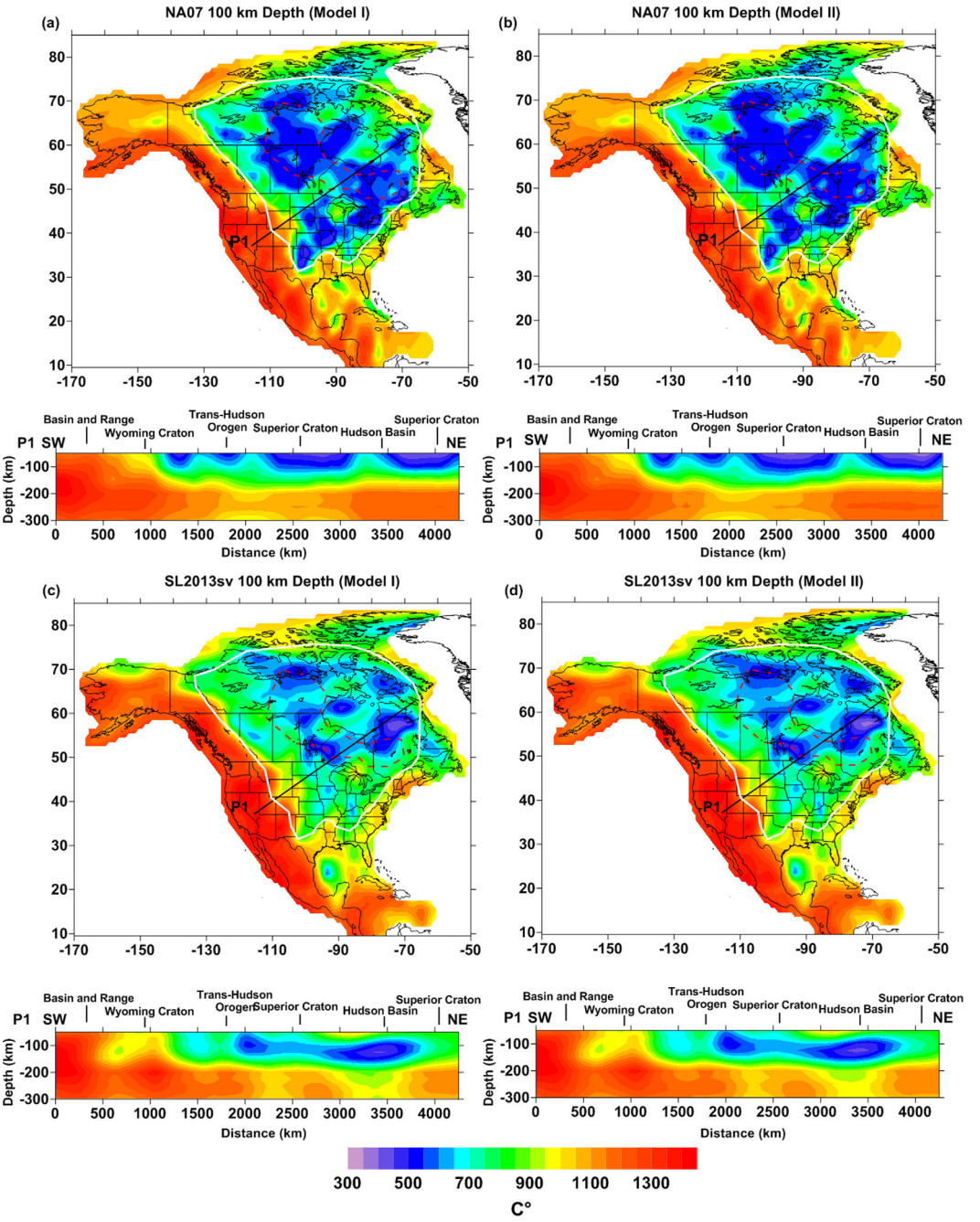

Figure 4. Estimated temperature (°C) in the NA upper mantle, after the last iteration at a depth of 100 km and along a cross section, derived from the inversion of (a and b) the regional seismic tomography model NA07 [*Bedle and van der Lee*, 2009] and (c and d) the global tomography model SL2013sv [*Schaeffer and Lebedev*, 2013]. White lines delimit the cratonic areas, where we estimated the temperatures, considering the compositional variations in the upper mantle. Red dashed lines delimit a representative area within the cratons for which the average temperature and residual density variations displayed in Figures 3a and 3b are estimated. For cratons, the composition changes according to two different depth distribution models of the residual density variations (Figure 3a) and anelasticity model Q3 [*Cammarano et al*., 2003] is used. Outside the cratons, the composition is uniform and corresponds to that of a "fertile" mantle [*McDonough and Sun*, 1995; *Griffin et al*., 2003] and anelasticity model Q4 [*Cammarano et al*., 2003] is used. See text for further explanation.

Lithgow-Bertelloni [2005], are estimated as a weight average of the Mg, Fe, and Ca (the latter in case of Gt) species (end-members) composing the four mineral phases considered in this study. More details on the method are provided in Part 1 [*Kaban et al*., 2014]. The composition used for the cratons changes in each point of the grid in terms of mineral fractions and Mg #, between two end-members rocks (Table 1), such that, as before explained, its density compensates the final residual ("compositional") density variations,

vertically distributed according to Model I and Model II (Figure 3a). The effect of anelasticity becomes significant at temperatures >900°C [*Jackson et al*., 2002] and can also be increased by the presence of fluids [e.g., *Karato and Jung*, 1998], but we assume that this effect is not very strong in the cold and generally dry lithospheric mantle of the cratons. Therefore, we use the smoothest anelasticity model (Q3, as specified in section 4) from those defined in *Cammarano et al*. [2003]. Outside the cratons, the uniform "fertile" composition and the anelasticity model Q4 used to estimate the initial temperatures remain unchanged. Therefore, we discuss only the new results shown by the final thermal models in the cratonic regions.

Temperatures estimated at a depth of 100 km and along a cross section are displayed in Figures 4a–4d. These estimates are up to ∼150°C higher in the Archean cratons, such as the Superior, Slave, and Churchill cratons, compared with the initial ones [cf., *Kaban et al*., 2014]. Consequently, the estimated difference between the hotter Proterozoic regions and the Phanerozoic NA cordillera is reduced. In fact, in the Proterozoic lithospheric mantle the increase of temperature after the correction is more modest (<50°C), according to its lower depletion. Since the difference in the residual density variations between the first and the last iteration, and thus in the compositional correction, is larger for NA07 than for SL2013sv (Figure 3a), the temperature increases more in NA07 compared to the initial values. The differences between the initial and the final composition tend to be reduced with depth and thus also the difference in temperature decreases in the deeper layers of the lithospheric mantle, becoming negligible below 250 km (see cross sections in Figures 4a–4d). Although we cannot easily define the depth of the thermal lithosphere beneath the cratons, we can observe that in all models below 200 km the lithospheric mantle becomes substantially warmer, indicating the proximity of the asthenosphere.

We note that the temperature difference between Model I and Model II (Figure 3a) is low (<50°C) for both NA07 (Figures 4a and 4b) and SL2013sv (Figures 4c and 4d). On the other hand, the difference in the final temperatures obtained by the two tomographic models in some parts of the cratons (e.g., the Proterozoic parts) does not change significantly with respect to that estimated between the two corresponding initial thermal models [*Kaban et al*., 2014]. Such a difference is similar to that between the initial and the final temperature models obtained using the same tomographic model. Therefore, the increase in temperature shown in the final models is comparable to the uncertainties in estimated temperature, which are related to the choice of the tomographic model. However, the final results, predicting a temperature >500°C at a depth of 100 km beneath most cratons, are more reliable than the initial ones, being in the range defined by the geotherms estimated from xenolith data [e.g., *Griffin et al*., 2004; *Pollack and Chapman*, 1977; *Hasterok and Chapman*, 2011]. In particular, we can observe that at a depth of 100 km in the Archean cratons the estimates provided by the NA07 model are close to the lower boundary of the range defined by xenolith data (∼600°C), while those of the SL2013sv model fall in the middle (∼750°C). In contrast, in the Proterozoic regions, the lowest values of NA07 are below the lower range defined by xenolith data (∼800°C), while those of SL2013sv also in this case fall in the middle (∼900°C). Therefore, the results obtained from the SL2013sv model appear to be more reliable according to the xenolith data. On the other hand, as discussed in sections 7 and 8, the reduced difference in temperatures between the Proterozoic and the Phanerozoic regions in the SL2013sv model, with respect to the NA07 model (Figures 4a–4d), results in the first model in an almost undepleted lithospheric mantle underlying the peripheral parts of the cratons. This finding is not supported by the results inferred from the xenoliths.

Temperatures estimated on the basis of surface heat flow measurements [*Artemieva*, 2006] are 100°C–200°C higher than our estimates and show a smooth lateral variation within the NA continent. The lowest values are found in the Canadian cratons surrounding Hudson Bay, and thus are not extended to the Slave craton in the north, neither to the south, as seen in our models. However, due to the scarcity and uneven distribution of the heat flow measurements in the Archean NA cratons [*Artemieva*, 2006], these results are not well constrained.

6. Effect of Compositional Variations on Residual Topography

In the companion study, Part 1 [*Kaban et al*., 2014], we estimated the residual topography (t_{res}), representing the part of topography that is uncompensated or over-compensated by the crustal structure, using NACr14 [*Tesauro et al*., 2014]. In order to identify the anomalous density distribution in the upper mantle, we suppressed the impact of other factors by filtering the local isostatic perturbations and removing the dynamic contribution given by the mantle heterogeneities below 325 km. Using the final thermal models (section 5),

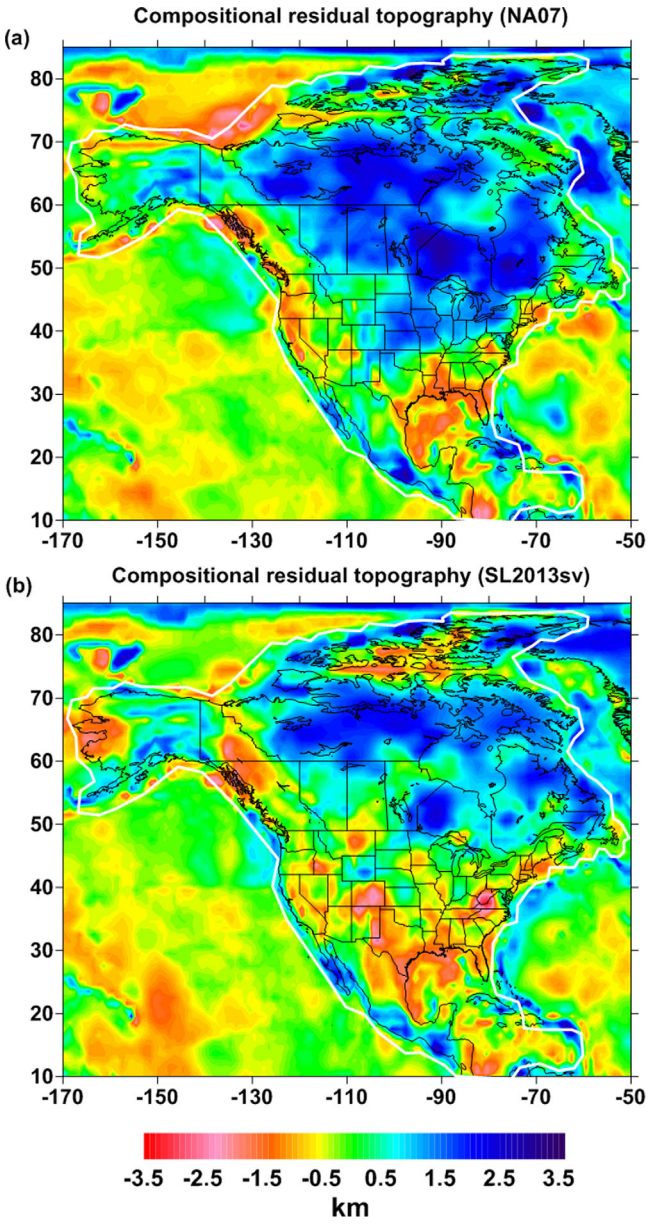

Figure 5. Final compositional component of the residual topography (t_{res}), estimated by subtracting from the total t_{res} [*Kaban et al.*, 2014] the final thermal component. The thermal fields are corrected for composition (Figures 4b and 4d) as obtained from the inversion of (a) the regional tomography model NA07 [*Bedle and van der Lee*, 2009] and (b) the global tomography model SL2013sv [*Schaeffer and Lebedev*, 2013]. Zero level corresponds to the reference density model. White contours delimit the study area. Outside the white contours the t_{res} is estimated using the global tomography model of *Ritsema et al.* [2011]. See text for further explanation.

corrected in the cratonic regions for the compositional variations due to depletion (section 4), we compute the dynamic topography induced by temperature variations above 325 km and subtract it from the total t_{res}. Therefore, we obtain the t_{res} only related to compositional changes. Potential uncertainties of the latter parameter depend on those affecting the total t_{res} (up to 0.6 km for the regions with thick crust and poor seismic coverage) and those related to the temperature estimation (an uncertainty in temperature of $\pm 100^{\circ}$C for a layer 100 km thick leads to an uncertainty of the dynamic topography of $\sim$0.37 km).

We display in Figures 5a and 5b, the compositional t_{res} for two of the four final thermal models (Figures 4b and 4d). Compositional t_{res} spans within a range of $\pm$3.5 km in both NA07 and SL2013sv, with the positive (negative) values related to negative (positive) density variations of the upper mantle due to compositional changes. The distribution of the compositional component of the t_{res} shows a prevalence of positive values in NA07, with the largest ones ($>$2 km) mostly observed in the cratonic areas (Figure 5a). In SL2013sv, the largest positive values are limited to some parts of the Canadian Shield, such as the Proterozoic platform, the northwestern part of the Superior craton, the Slave and the northern part of the Churchill craton (Figure 5b). Therefore, these results point to the existence of a buoyant lithospheric mantle at least in a part of the Archean cratons, on account of its strong depletion in high-density components. However, since the same areas are characterized by weaker positive values ($<$1.5 km) of the total t_{res} [*Kaban et al.*, 2014], we can deduce that a part of the compositional t_{res} is compensated by the counteracting effect of low temperatures (Figures 4b and 4d). The largest differences between the two models are observed in the central U.S. and the southern part of Canada, corresponding to the western and more deformed part of the NA cratons (e.g., Trans-Hudson Orogen and the Rocky Mountains) and to transitional areas (e.g., the Colorado Plateau). In these regions, the positive values observed in NA07 ($>$1.5 km) correspond to negligible ($<$0.5 km) or even negative estimates in SL2013sv (up to $-$1.5 km), with the exception of the inner core of the Colorado Plateau, which also in NA07 shows negative compositional t_{res} (~ -1 km). Therefore, NA07 would generally indicate a lithospheric mantle that has been moderately depleted, as

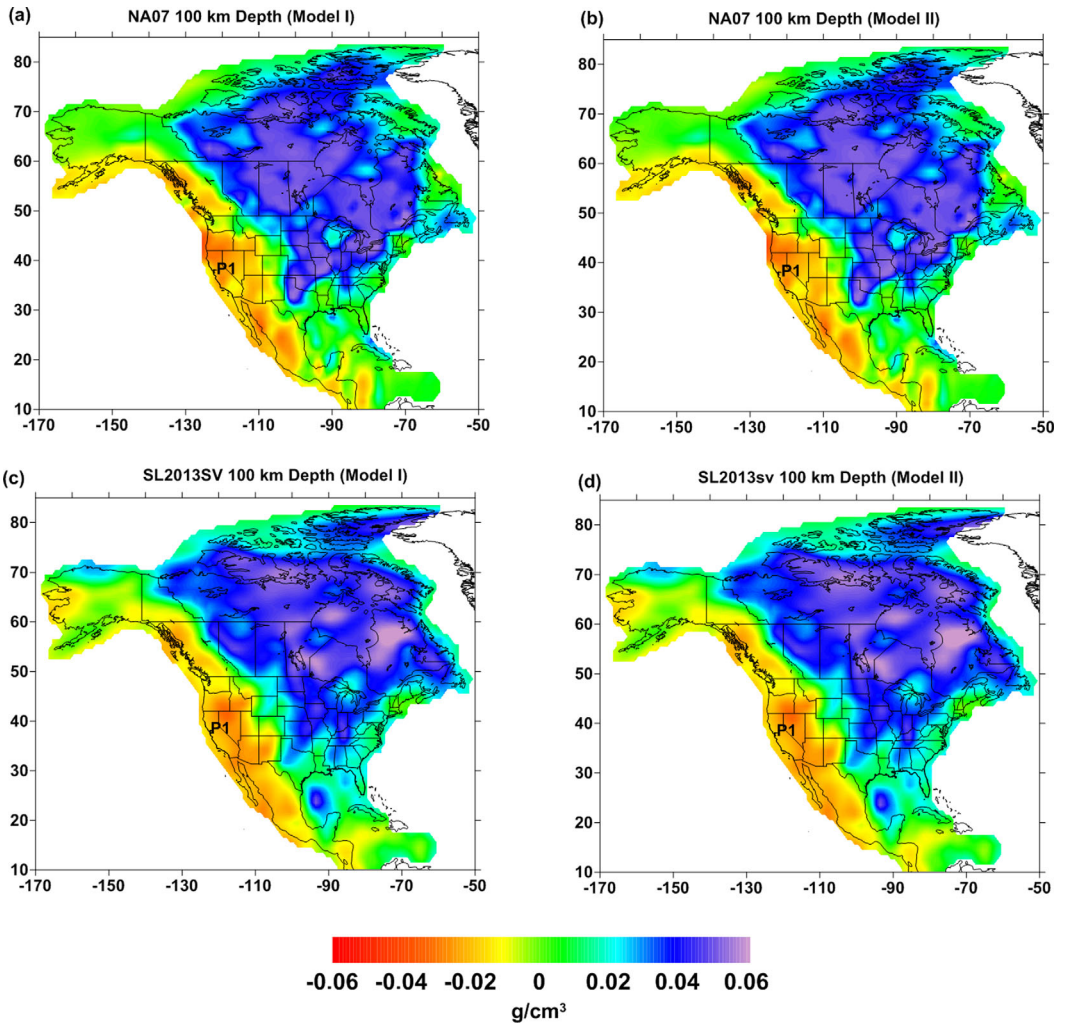

Figure 6. Thermal density variations in the NA upper mantle at a depth of 100 km estimated using (a and b) the regional tomography model NA07 [*Bedle and van der Lee*, 2009] and (c and d) the global tomography model SL2013sv [*Schaeffer and Lebedev*, 2013], according to two different depth distribution models of the residual density variations (Model I and Model II). See text for further explanation.

expected for its age (mostly Proterozoic), and which buoyancy would raise the topography. In contrast, in SL2013sv the negative values would indicate the presence of small high-density bodies that might cause subsidence. However, the total t_{res} in these areas is weakly or largely positive (>2 km) [*Kaban et al.*, 2014], indicating that effects of possible high-density bodies are overcompensated by those exerted by relatively high temperatures (Figures 4b and 4d).

In the off-craton regions, such as the Appalachians and Grenville Province, both models show negligible (more often in NA07) or negative values (<-1 km) for residual topography, t_{res}. The latter might be related to the presence of fragments of slab [e.g., *Thomas*, 1989], as discussed further in the next section. However, also in these off-craton areas the total t_{res} is generally positive (up to ~1 km) [*Kaban et al.*, 2014], indicating that the effect of temperature, which in the lithospheric mantle is higher than beneath the cratons, prevails. In contrast, the negative compositional t_{res} (up to ~ -1.5 km) identified in both models in most part of the Gulf of Mexico and along the NA southern margin seems to be a more robust feature, which might be produced by a shallow high-density body, possibly responsible for the subsidence of the Gulf of Mexico [*Mooney and Kaban*, 2010]. In SL2013sv, the negative compositional t_{res} along the NA southern margin extends northward up to Colorado, including the southern part of the Rocky Mountains (~ -2 km). Although the subduction of high-density bodies such as eclogite might cause the cooling of the overlying upper mantle, the temperatures in these regions (Figures 4a–4d) are high enough to overcompensate their compositional effect, as we can deduce by the large positive values of the total t_{res} (in some parts >2 km) [*Kaban et al.*, 2014].

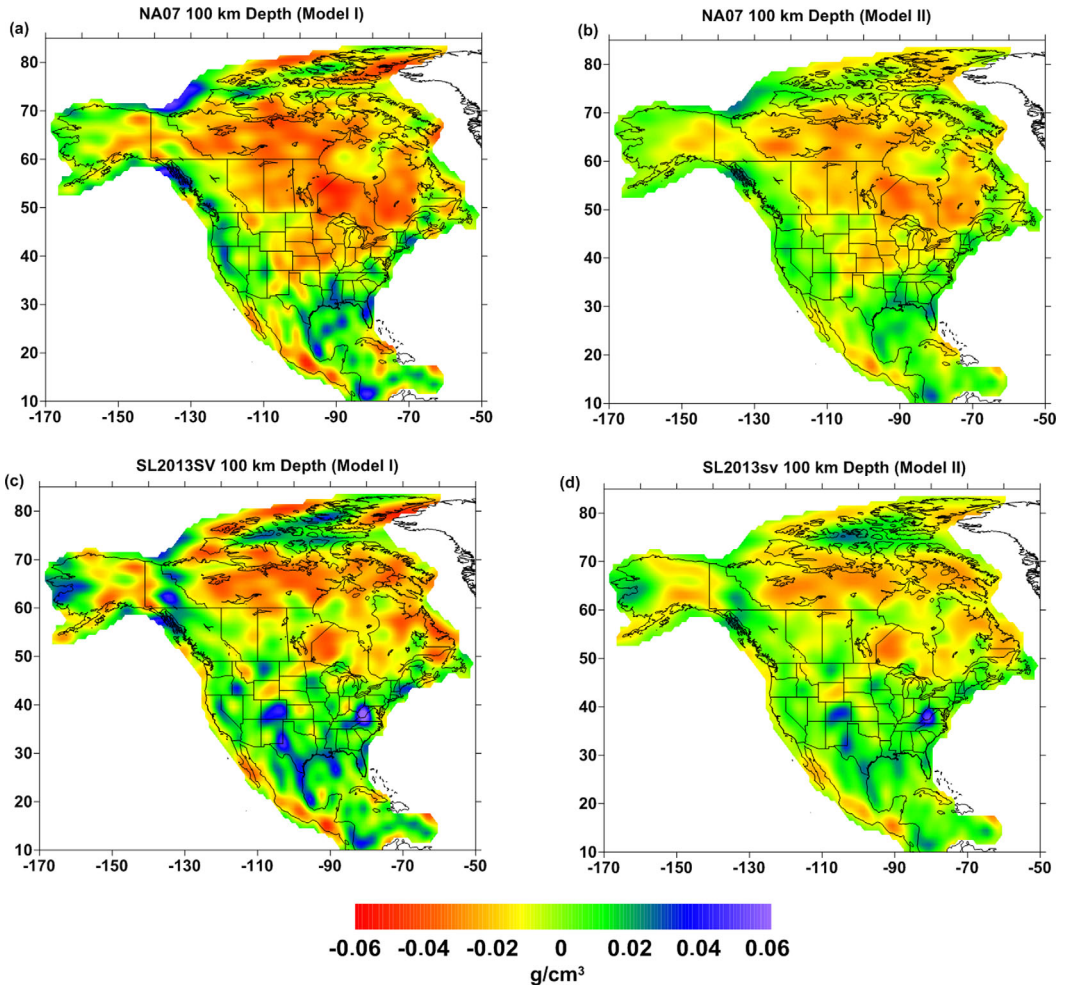

Figure 7. Compositional density variations in the NA upper mantle at a depth of 100 km estimated using (a and b) the regional tomography model NA07 [*Bedle and van der Lee*, 2009] and (c and d) the global tomography model SL2013sv [*Schaeffer and Lebedev*, 2013], according to two different depth distribution models of the residual density variations (Model I and Model II). See text for further explanation.

As discussed in our companion study, Part 1 [*Kaban et al.*, 2014], the NA Cordillera is characterized by the largest positive values of the total t_{res} (>3 km), since the high temperatures, related to its location in a back-arc tectonic setting [e.g., *Hyndman and Currie*, 2011], tend to raise the topography. We can observe that the compositional t_{res} in both models is positive (>2 km) along the western margin of Mexico and southern margin of Alaska. However, a compositionally buoyant lithospheric mantle, related to depletion as in the Archean cratons is unlikely in these Phanerozoic regions, except in case the upper mantle of these regions have experienced a second stage of melting (e.g., associated with the subduction processes) [*Pearson and Witting*, 2008]. Nor can these features be explained with other effects (fluids and/or partial melts) since these have a negligible influence on density [e.g., *Afonso and Schutt*, 2012]. Therefore, these positive anomalies might be the result of underestimated temperatures, possibly on account of lower resolution of the tomography models in this region [*Bedle and van der Lee*, 2009], which might cause an uncertainty in temperature of up to 150°C, when anelasticity is not activated (i.e., for T < 900°C) [*Kaban et al.*, 2014]. In other parts of the Western NA margin (e.g., in Cascadia) the negative values of the compositional t_{res} (up to about −1.5 km) might reflect the effects of the downwelling produced by the subducting Juan de Fuca plate [e.g., *Becker et al.*, 2014].

7. Thermal and Compositional Component of the Upper Mantle Density

The complete density distribution in the NA upper mantle is estimated in Part 1 [*Kaban et al.*, 2014] by inversion of the residual mantle gravity field and residual topography. Here we estimate the thermal

component of the density variations using the final thermal models, corrected for the compositional changes in the cratonic regions (Figures 4a–4d). By subtracting the thermal density variations from the total one, we estimate the density changes due to composition.

The final thermal density variations for a depth of 100 km (Figures 6a–6d), span from -0.04 to 0.055 g/cm^3 in NA07 and from -0.033 to 0.065 g/cm^3 in SL2013sv, respectively. We notice that the results reflect the temperature distributions obtained from the inversion of the tomographic models (Figures 6a–6d), and thus the division of the NA continent between the Western Phanerozoic Cordillera and the stable old cratons in the central and eastern part of the continent. In fact, we can observe that positive and negative density variations are found in the cratonic and off-cratonic regions, with low and high temperatures, respectively. An exception is given by the Archean Wyoming craton, which is characterized by slightly positive density variations, on account of its high thermal regime. We can also notice that the difference in the results obtained using either Model I or Model II for the same tomographic model is negligible. According to the initial tomography models, the positive values in the cratonic regions persist up to a depth of 200–250 km. Below this depth, the anomalies tend to be close to zero or slightly positive.

The final compositional component of the density variations estimated at a depth of 100 km is displayed in Figures 7a–7d. According to Model I, the compositional density anomalies are within ± 0.055 g/cm^3 in NA07 and span from -0.055 to 0.07 g/cm^3 in SL2013sv (Figures 7a and 7c). When the residual density variations are vertically distributed according to Model II, the range of the anomalies is reduced to ± 0.035 g/cm^3 in NA07 and spans from -0.035 to 0.055 g/cm^3 in SL2013sv. As was mentioned above, this is likely a result of the damping in the joint inversion of the residual gravity and topography (Kaban et al., submitted manuscript, 2014). We note that in NA07 the negative values are dominant in the cratonic regions and tend to prevail in the entire continent. In contrast, in SL2013sv the negative and positive values are equally distributed in the continent, with a prevalence of negative values in the cratonic areas. The largest negative anomalies (<-0.030 g/cm^3), pointing to a strong depletion of the uppermost mantle, in both NA07 and SL2013sv, are mostly observed in the Archean part of the Canadian Shield, such as the central part of the Slave craton and the northern part of the Superior and Churchill craton. Other cratonic regions and in particular those of Proterozoic age (e.g., the Rocky Mountains), are characterized by lower negative values (>-0.025 g/cm^3) in NA07 or even positive (up to 0.030 g/cm^3) in SL2013sv, predicting a lithospheric mantle weakly depleted or locally characterized by high-density bodies.

In the areas outside the cratons, the density anomalies are vertically distributed, according to the same models for the depth distribution of the residual density variations used in the cratonic regions. We used Model I in off-cratons regions as well, in order to compare their anomalies with those estimated in the cratons. In fact, as previously discussed, in the Phanerozoic mantle the anomalies are likely to be due to compositional variations not related to depletion. In any case, we do not have petrological constraints to infer a realistic vertical distribution of these anomalies, different from that identified by the tomographic models. We can observe that for both NA07 and SL2013sv there are some positive anomalies (up to $\sim$0.02 g/cm^3, locally reaching $\sim$0.05 g/cm^3) in the Grenville and Appalachian province and close to the suture between these provinces. As observed by *Mooney and Kaban* [2010], these positive anomalies might correspond to remnant slab fragments in the uppermost mantle, as a consequence of the closing of the paleo-Atlantic during the early stages of the Appalachian orogeny [e.g., *Thomas*, 1989]. The crust of fossilized subducted slabs, which have undergone a basalt-ecolgite transformation, will increase in density from $\sim$3.30 to 3.40–3.50 g/cm^3 [e.g., *Kopylova et al*., 2004]. *Van der Lee et al*. [2008] hypothesize that the lack of high velocities in this region is due to the hydration of the upper mantle (an inference that is also supported by magnetotelluric measurements) [e.g., *Kurtz and Garland*, 1976] from subducted slabs, which might have facilitated the basalt-eclogite metamorphic transformation. In the Gulf of Mexico and along the southern margin of the continent a chain of small positive anomalies (0.02–0.035 g/cm^3) are observed in NA07, while in SL2013sv the same anomalies have a smaller areal extent. Since these anomalies do not correspond to fast seismic velocities in the two tomographic models, we can interpret them as due to bodies of eclogite, usually seismically indistinguishable from a peridotite, located in the shallowest part of the upper mantle. The results obtained using the two tomographic models differ along the border between New Mexico and Texas and between the northwestern part of the Colorado Plateau and the southern Rocky Mountains. In this part of the continent, the negative density variations (~ -0.25 g/cm^3), estimated in NA07, correspond in SL2013sv, to large positive values, which reach two maxima of $\sim$0.04 g/cm^3 (Figures 7c and 7d). Therefore, the

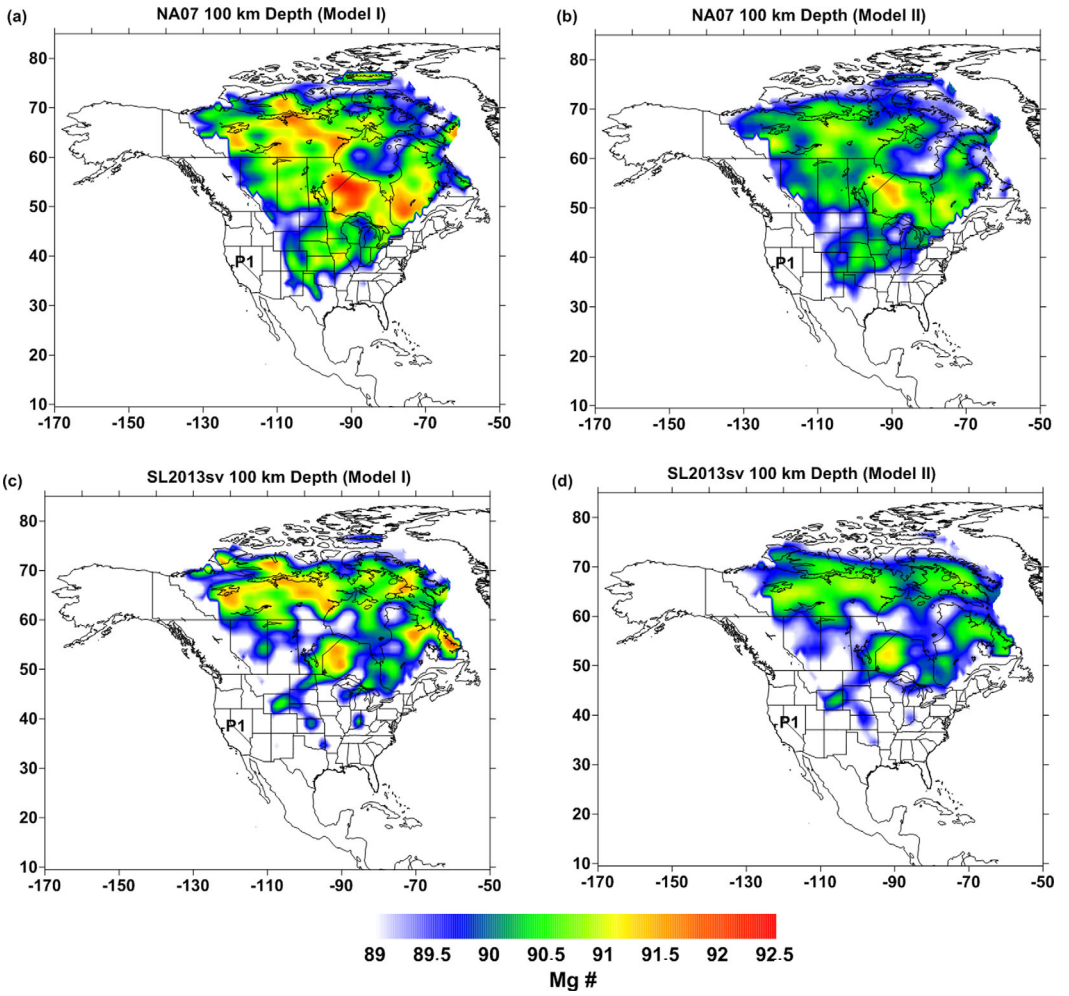

Figure 8. Depletion variations in terms of Mg # (100 × Mg/(Mg + Fe)) in the Archean and Proterozoic NA upper mantle at a depth of 100 km estimated using the regional tomography model NA07 [*Bedle and van der Lee*, 2009] and the global tomography model SL2013sv [*Schaeffer and Lebedev*, 2013], and according to two different depth distribution models of the residual density variations (Model I and Model II). See text for further explanation.

lithospheric mantle, close to the cratonic border should be weakly depleted, if we consider the results obtained in NA07 realistic, while in the opposite case, a couple of high-density bodies should be present in its uppermost part. *Mooney and Kaban* [2010] found results similar to those of SL2013sv, observing a broad positive N-S oriented anomaly. They interpreted this positive anomaly as a piece of slab derived from the slab breakoff, occurring during the evolution of the NA Cordillera [*Hildebrand*, 2009] or as a result of the advection of the lithospheric mantle induced from the eastward-directed flat slab subduction [e.g., *Bird*, 1988]. However, regardless of the origin of these anomalies, their effect on the possible deflection of the topography is negligible, being overcompensated, as discussed in the previous section, by that of the high temperatures. We note that the results obtained from the two tomography models, although diverging in parts of the cratons, are not necessarily in conflict. In fact, we speculate that the lithospheric mantle is likely weakly depleted, as displayed in the NA07 model, and at the same time small high-density bodies, visible in the SL2013sv model, are locally present.

In the western part of North America, the largest negative density variations (up to -0.05 g/cm^3) are estimated in both tomographic models in Alaska and along the western margin of Mexico, indicating a buoyant upper mantle. As discussed in the previous section, these anomalies are likely to be an artifact, since in the area with lower resolution in the tomography models the uncertainty in residual densities could be $\sim$0.01 g/cm^3 [*Kaban et al.*, 2014]. In other parts of NA Cordillera, the density variations are negligible or weakly positive (usually $\sim$0.01 g/cm^3), indicating that the effect of the high temperatures can explain the

total density variations. Larger positive anomalies are observed in the Sierra Nevada and Cascadia areas ($>$0.020 g/cm^3) in NA07 and possibly reflect the effect of the high-density subducting Juan de Fuca plate.

The results of the inversion indicate that the cratonic lithospheric mantle tends to have a uniform composition below 200 km. In fact, in most of cases, the negative density anomalies are significantly reduced below this depth, as we would expect in close proximity with the asthenosphere.

8. Depletion Variations in the Lithospheric Mantle Under the Craton

As previously explained, we compensate for the negative values of the residual density variations estimated in the cratonic regions by varying the Mg # and the percentage of the mineral constituents within a range given by the two end-members rocks (Table 1). In Figures 8a–8d, we display the compositional heterogeneity in terms of Mg # in the cratonic lithospheric mantle, after the last iteration, at a depth of 100 km. Mg # spans from 89 to 92.4 in NA07 and from 89 to 91.9 in SL2013sv (Figures 8a–8d). We can observe that the most depleted regions are the Archean cratons (Table 2), such as the northwestern part of the Superior craton, the central part of the Slave and Churchill craton (Table 2), in both NA07 and SL2013sv. The Wyoming craton is slightly depleted in both models (Mg # up to 90.5), supporting the hypothesis that part of the lithospheric mantle has been effectively replaced by fertile mantle (or refertilized by infiltration of iron-rich basaltic melts) during Phanerozoic tectonic activity [e.g., *Carlson et al*., 2004]. We can notice that in SL2013sv the depletion mainly occurs in the Archean Canadian Shield, while in NA07 it is extended toward the central and eastern part of the U.S., encompassing most of the Proterozoic terranes, up to the eastern border of the Colorado Plateau. The latter, although containing a large portion of fertile lherzolite, might be locally strongly depleted (Mg # $>$92), based on a lithospheric mantle composition-depth model constructed from xenoliths [e.g., *Griffin et al*., 2004]. Other Proterozoic areas are in general moderately depleted (Mg # $\sim$91) in NA07 and almost undepleted (Mg # $=$89) in SL2013sv, while few maxima (Mg # $>$91) are observed in both models in the Canadian platform. The results based on the interpretation of xenolith data are in agreement with those estimated using the NA07 tomographic model. In fact, they predict a Mg # of 91–92 [*Griffin et al*., 2004] in the lithospheric mantle of the Proterozoic areas, on account of its partial fertilization or a lower degree of melt depletion.

We also observe that when the compositional densities are vertically distributed according to Model I (Figure 3a), the cratonic regions with higher depletion (Mg # $>$91) are more extensive than in the other case. In fact, according to Model II, there is only one large anomaly in both NA07 and SL2013sv, coinciding with the northwestern part of the Superior craton, while the lithospheric mantle of other cratonic regions appears compositionally more uniform, and only weakly vertically and laterally depleted. Since this is possibly the result of the damping, Model I likely provides more reliable values. The large value of Mg # ($\sim$92.4) estimated for the Superior and the Slave cratons according to NA07 and Model I (Figure 8a), is in agreement with the average value inferred from xenolith data [e.g., *Griffin et al*., 2004; *Aulbach et al*., 2007]. The nucleation of the Slave craton occurred through partial melt at intermediate depth (6–3 GPa) [*Herzberg*, 1999; *Aulbach et al*., 2007], resulting in a strongly depleted uppermost mantle ($<$150 km), with respect to its lower part (150–240 km). The shallow, ultradepleted lithospheric mantle may have been generated in a collisional setting [*Griffin et al*., 1999] and, according to *Aulbach* [2012], at excess potential temperatures, experiencing large melting intervals. In contrast, the lower part of the lithospheric mantle may have been formed from subcretion of plumes beneath a preexisting lithospheric lid, which produces less depleted residues because of narrower melting intervals [*Griffin et al*., 2004; *Aulbach*, 2012]. Other studies [e.g., *MacKenzie and Canil*, 1999] indicate that the depletion of the Slave craton can be locally stronger (Mg # $\sim$94), but the tomography models used are too coarse to detect these local heterogeneities. On the other hand, the results from Model II (Figures 8b

Table 2. Maximum Values of Mg # (100 $\times$ Mg/(Mg + Fe)) Estimated in the Archean and Proterozoic NA Upper Mantle Using the Regional Tomography Model NA07 [*Bedle and van der Lee*, 2009] and the Global Tomography Model SL2013sv [*Schaeffer and Lebedev*, 2013] and Using Two Different Depth Distribution Models of the Residual Density Variations[a]

	Archean	Proterozoic
Mg # NA07 Model I	92.4	91.5
Mg # NA07 Model II	91.5	91
Mg # SL2013sv Model I	91.9	91.5
Mg # SL2013sv Model II	91.2	91

[a]See text for further explanation.

and 8d), predicting an almost linear decrease of depletion with depth (Figure 3a), might represent the composition of the lithospheric mantle of other cratonic regions not characterized by a shallow ultradepleted lithospheric mantle [*Griffin et al*., 2004]. In the lowermost part of the lithospheric mantle (>200 km), the residual density variations (Figure 3a) drops in all the models presented below a value of −0.016 g/cm^3, indicating a general weak depletion (Mg # <90).

Conclusions

Using a regional (NA07) and a global (SL201sv) tomography model and gravity data, we apply the iterative technique described in Part 1 [*Kaban et al*., 2014], to simultaneously estimate temperature and compositional variations occurring in the NA lithospheric mantle. We vertically distributed the mantle residual density variations, obtained by subtracting from the total density the thermal component evaluated from the initial thermal fields, according to two models. The first one (Model I) reproduces the composition of a lithospheric mantle with stronger chemical depletion in its shallowest part (<150 km). In the second model (Model II), based on the direct inversion of the residual gravity and residual topography, the residual density variations (and thus the depletion) are almost linearly distributed [*Kaban et al*., 2014]. The negative residual densities were compensated by the density of a rock with a larger Mg # and depleted in Gt and CPX and the temperature was reestimated using the new composition iteratively. From the results obtained, consisting of four thermal and compositional models, two for each tomography model (Na07 and Sl2013sv) and type of vertical distribution of the residual densities (Model I and Model II), we conclude that:

1. Differences in the estimates of temperature and composition of the cratonic lithospheric mantle provided by the two tomography models are stronger than those provided by the two types of distribution of the residual densities using the same tomography model. Hence, the seismic tomography model that is adopted plays a very significant role when estimating cratonic temperature and composition from geophysical data.
2. Temperatures under the Archean cratons are about 150°C higher in our models compared with one that assumes a lateral and vertical uniform "fertile" composition and are within the range defined by the geotherms constructed using xenolith data. The higher temperatures cause a decrease of the residual density variations <0.01 g/cm^3. In contrast, final temperatures estimated in the Proterozoic regions remain almost unchanged with respect to the initial temperatures, and thus also the difference between the results obtained using the two seismic tomography models remains relatively high in some parts of the lithospheric mantle. The temperatures obtained from the SL2013sv model, being higher in these regions (up to 200°C) than those estimated by the NA07 model, are in agreement with those predicted by xenolith data.
3. Using the tomographic model NA07, the negative density values are dominant in the cratonic regions and tend to prevail in the entire continent. In contrast, in the tomographic model SL2013sv the negative and positive values are equally distributed within the continent, with a prevalence of negative values in the cratonic areas. Within the cratons the buoyancy of the lithospheric mantle due to the chemical depletion tends to raise the topography, but this effect is mostly balanced by that exerted by the cold temperatures.
4. The largest differences between the results obtained from the two tomography models are found in more deformed parts of the NA cratons of Proterozoic age (e.g., THO, Rocky Mountains, and Colorado Plateau). These areas are characterized by lower negative values (>−0.025 g/cm^3) in NA07 or even positive (up to 0.040 g/cm^3) in SL2013sv, predicting a lithospheric mantle weakly depleted (Mg # ∼91 or more) or locally characterized by high-density bodies. The latter might be interpreted as the effect caused by a piece of slab derived from the slab breakoff occurring during the evolution of the NA Cordillera [*Hildebrand*, 2009] or by the advection of the lithospheric mantle induced from the eastward-directed flat slab subduction [e.g., *Bird*, 1988]. However, the results based on the interpretation of xenolith data are in agreement with those of model NA07, since they predict a weak depletion in the Proterozoic regions [e.g., *Griffin et al*., 2004].
5. The largest negative anomalies (<−0.030 g/cm^3), pointing to a strong depletion of the uppermost mantle (Mg # ∼92), in both model NA07 and model SL2013sv, correspond to parts of the Archean cratons, such as the northwestern part of the Superior craton and the central part of the Slave and Churchill craton. The largest values of Mg # estimated in Model I are in agreement with the average values obtained from the interpretation of xenolith data [e.g., *Griffin et al*., 2004]. The results from Model II, predicting an almost linear decrease of depletion with depth, might reflect the composition of the lithospheric mantle of other parts of the cratons that are not characterized by a shallow ultradepleted layer.

6. Temperatures are estimated according to a uniform "fertile" composition in the off-cratons regions. Prominent, positive compositional density anomalies, found beneath the Gulf of Mexico and along the southern NA margin ($\sim$0.02 g/cm^3) are interpreted as the effect of high-density bodies (e.g., eclogite in the shallow upper mantle). Additional positive density anomalies, close to the suture between the Grenville and the Appalachian province and in SL2013sv in the southern Rocky Mountains, may represent a high-density oceanic slab, formed during the early stages of the evolution of the Appalachians and of the NA cordillera. The central part of the Western Cordillera is also characterized by positive compositional density anomalies ($>$0.020 g/cm^3), possibly reflecting the effect of the subducting slab, which tends to cause, as in the other cases, a deflection of the topography (~-1.5 km). However, the latter effect is overcompensated by that produced by the high temperatures.
7. Comparison of the results obtained using two tomography models with those obtained from previous studies indicate that a consideration of the two models yields a more complete picture of the possible compositional variations of the NA lithospheric mantle. In fact, in the Proterozoic regions the depletion is likely weak, as displayed in the NA07 model, and the small high densities bodies visible in the SL2013sv model might also be present.

Appendix A: Effect of Composition on the Physical Properties of the Upper Mantle

The change of Mg # in minerals strongly influences seismic velocities and density [e.g., *Matsukage et al*., 2005]. To investigate the effect of its variations on the physical parameters of the main minerals composing the upper mantle, we compute density and anharmonic compressional and shear velocities for the most common range of Mg # observed in the peridotite (89–94), at standard T and P (STP) conditions. To this purpose, we use the density and the elastic modulus of the mineral phases defined in *Cammarano et al*. [2003].

The results displayed in Figures A1a–A1c show that density and both shear and compressional velocity of each mineral are inversely and positively correlated with Mg #, respectively. Since the density and shear modulus of minerals are more sensitive to Mg # variations in comparison with the bulk modulus [e.g., *Lee*, 2003], changes in Mg # have larger effects on shear wave velocities than on compressional-wave velocities (Figures A1b and A1c). The contribution given by Ol to density (ρ) and shear velocity (V_s) variations ($\Delta\rho = \sim-0.012$ g/cm^3, $\Delta V_s = 0.018$ km/s) by increasing Mg # is significantly larger compared to the other minerals composing a peridotite. However, the abundance of Gt, which has the highest density and seismic velocity, strongly influences the physical properties of the bulk rock [e.g., *Schutt and Lesher*, 2010].

As pointed out in section 2, petrological analyses on natural samples showed that variations in the percentage of mineral phases are usually accompanied by changes in Mg # [e.g., *Lee*, 2003]. However, in the tests we have performed, displayed in Figures A2a–A2c and A3a–A3c, we isolate and describe the effects of Mg # and mineral fraction variations, in order to estimate the effect of composition on density and seismic velocity due to these two components separately.

Figure A2a displays estimates of density versus Mg # of two bulk rocks at the STP conditions, with the same mineral fractions defined for the two end-member compositions considered in this study, "fertile" and "refractory," respectively (Table 1). Since Ol and OPX are the two minerals more sensitive to Mg # variations, the density of the "refractory" mantle, more enriched in these minerals, varies slightly more strongly than that of "fertile" mantle, when the Mg # changes. The increase of Mg # by five units (from 89 to 94) causes an average density variation in the bulk rock of $\sim$0.05 g/cm^3 ($\sim$1.5%), similar to those estimated in previous studies [e.g., *Nolet and Zielhuis*, 1994; *Deschamps et al*., 2002]. The difference in density between the two bulk rocks for the same Mg # slightly increases when large values of Mg # are assumed, but on average is about $\sim$0.03 g/cm^3 ($\sim$0.9%). Therefore, as discussed below in more detail, the change of Mg # in the rocks has a greater effect on density (almost the double), compared to that of variations in mineral fractions.

As for the density, the effect of Mg # on the P and S velocities variations is larger for the "refractory" than for the "fertile" composition (Figures A2b and A2c). We can observe that, in agreement with previous studies [e.g., *Nolet and Zielhuis*, 1994; *Deschamps et al*., 2002], the increase of Mg # by 5 units (from 89 to 94) causes in both types of rocks an average increase of P and S wave velocity of $\sim$1% and 1.3%, respectively. Compensating this increase in seismic velocity would require a temperature increase of $\sim$200°C (without considering the effects of anelasticity). In addition, we can observe that the P velocity of the "refractory"

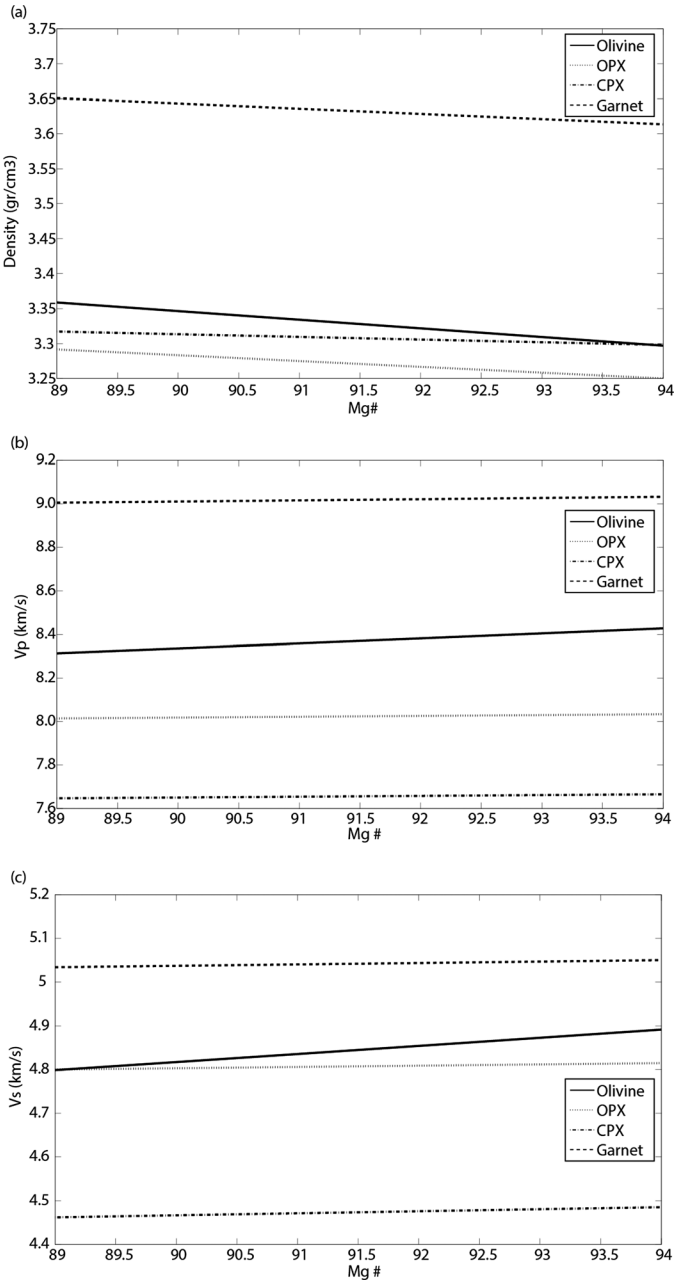

Figure A1. (a) Density, (b) compressional-wave, and (c) shear wave seismic velocity variations of the main minerals of the upper mantle up to a depth of 300 km versus Mg # (100 × Mg/(Mg + Fe)). See text for further explanation.

composition is lower than that of the "fertile" composition and such a difference decreases with the increase of the Mg #. In contrast, the *S* wave velocity of the "refractory" composition is on average larger than that of the "fertile" composition and tends to increase with an increase of the Mg #.

We investigate the effects on mantle density and seismic velocities, induced by various compositional changes and varying *P* and *T* conditions. To this purpose, we estimate densities and seismic velocity variations in rocks with the same mineral fractions of the two end-member peridotites, for a *P* of ∼1.4 and ∼9.8 GPa, respectively, corresponding to shallow (50 km) and deep (300 km) upper mantle, a large *T* range (0°C–1800°C) and Mg # ranging from a minimum of 89 and a maximum of 94 (Figures A3a–A3c), using the equations of *Stixrude and Lithgow-Bertelloni* [2005]. We can observe that the difference in density between these two types of rocks is not very sensitive to these variations (Figure A3a). This difference slightly increases by

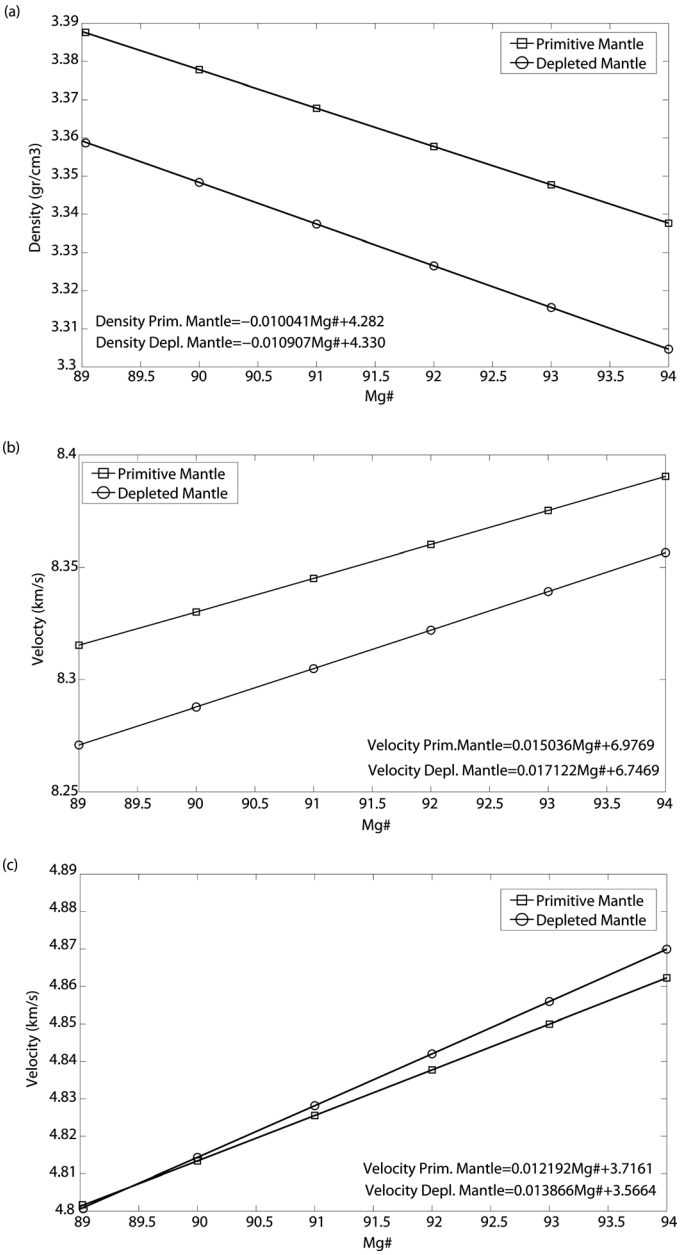

Figure A2. (a) Density, (b) compressional, and (c) shear velocity variation with respect to Mg # (100x × Mg/(Mg + Fe)) of the STP peridotite having a "fertile" and a "refractory" composition, respectively. See text for further explanation.

increasing in both rocks the Mg #, on account of the large sensitivity of Ol to density. The difference in density between the two rocks reaches, on average, a maximum value of ∼0.08 g/cm^3 (∼2.3%), when they have a difference of 5 units in Mg #.

In contrast, the difference in seismic velocity between the two rocks is not constant with varying *P* and *T* conditions (Figures A3b–A3c). As previously discussed, the compressional velocity is higher in the "fertile" than in the "refractory" composition and such a difference increases by decreasing *P* and increasing *T* (Figure A3b). The difference in the shear velocities are lower, being close to zero at a depth of 50 km and at temperature <600°C (Figure A3c). At higher *T*, the velocity of the "fertile" composition becomes slightly higher in respect to the "refractory" mantle rock. Such an increase of velocity, at a depth of 300 km occurs at lower *T* (∼300°C) (Figure A3c). The variations observed are due to the larger thermal derivative of the shear modulus of Ol in respect to those of the other minerals [*Cammarano et al.*, 2003]. Since both shear

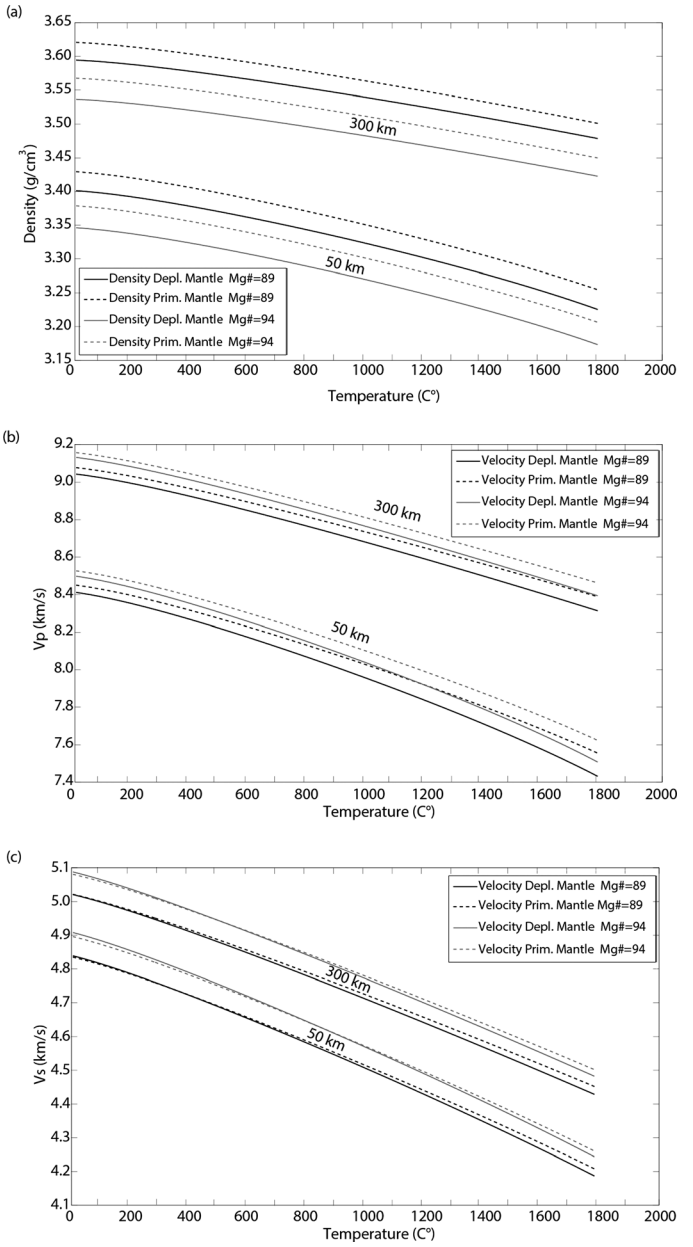

Figure A3. (a) Density, (b) compressional, and (c) shear velocity variation of "fertile" and "refractory" peridotites having a Mg # (100 × Mg/(Mg + Fe)) 89 and 94, with *T* (0–1800°C) and *P* of ~1.4 and ~9.8 GPa, corresponding to a depth of 50 and 300 km, respectively. See text for further explanation.

velocity and density of Ol are quite sensitive to the Mg # (Figure A1b), the increase of the latter in both types of rocks causes a small increase of velocity in the "refractory" composition, being richer in this mineral. However, since these variations are small, we conclude that the only lithological changes between the two end-members compositions have a negligible role in varying the velocities of the bulk rocks.

We evaluate now the combined effects of Mg # and variations of mineral fractions on density and shear velocity. To this aim, we estimate the density and velocity variations in a rock, whose lithological and chemical composition changes linearly, within the range defined by the two end-members. We can observe that the relationship dρ/dMg # at STP conditions ($\rho = -0.0166$ Mg # + 4.87) is in the range obtained in previous studies (Figure A4a) based on xenolith analyses ($\rho = -0.0144$ Mg # + 4.66 in the study of *Lee* [2003] and $\rho = -0.0191$ Mg # + 5.09 in the study of *Jordan* [1988], respectively). The empirical relationship between bulk velocity and bulk Mg # ($V_s = 0.0137$ Mg # + 3.58) is slightly less steep compared to the previous one

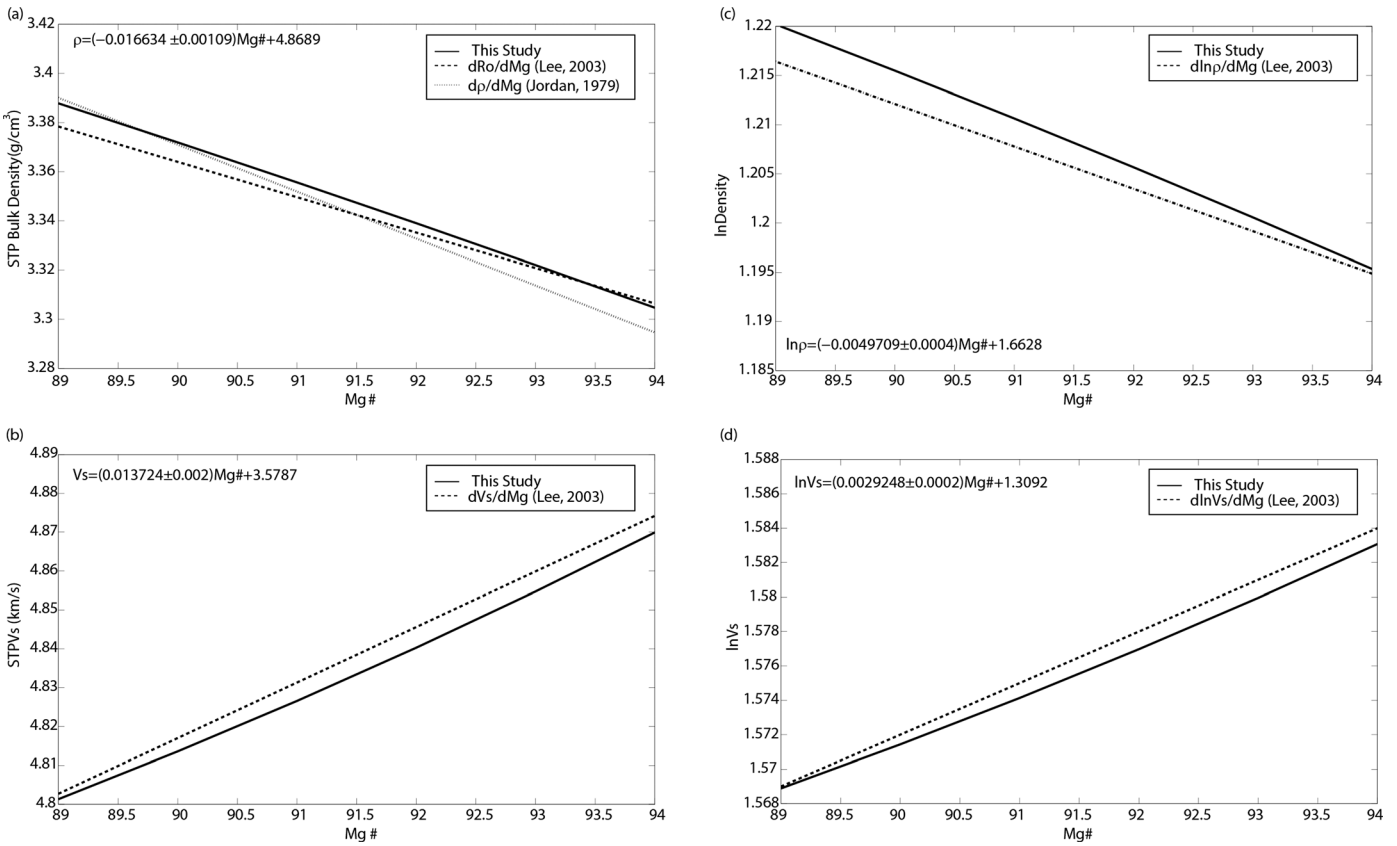

Figure A4. Continuous black lines show the relationship between Mg # and (a) density; (b) seismic velocity; (c) natural logarithm of density; (d) natural logarithm of seismic velocity of rocks having a composition spanning between a "fertile" and a "refractory" mantle versus Mg # (100 × Mg/(Mg + Fe)). Dotted black and gray lines show the same relationship estimated in previous studies. See text for further explanation.

(V_s = 0.0143Mg # + 3.53) obtained in the study of *Lee* [2003], as well as the relationships dlnρ/dMg # and dlnV_s/dMg # (Figures A4b–A4d). Based on the value of derivative dρ/dMg # as above discussed, we estimate that a minimum amount of depletion, given by an increase of 0.1 in Mg # and a change in the corresponding fractions of the main minerals, with respect to the "fertile" end-member (Table 1), is compensated by a density variation of ∼0.0016 g/cm^3 (section 4).

Despite the agreement found between our results and those obtained from natural samples, we should also keep in mind that other rocks with a lithological and chemical composition different from those here defined may fit well the relationship between bulk density/velocity and Mg # given by the suite of xenoliths displayed in *Lee* [2003]. However, our aim is to explain the origin of the lithospheric mantle heterogeneity using compositions compatible with those representatives of the typical suite of depletion.

Acknowledgments
We thank Sonja Aulbach and the Editor Cin-Ty A. Lee for their extensive reviews that have greatly improved the manuscript. This study was funded by an Alexander von Humboldt Foundation postdoctoral grant and research award, GeoForschungsZentrum, Potsdam, Utrecht University, the Netherlands Research Centre for Integrated Solid Earth Science (ISES), and the USGS National Earthquake Hazards Reduction Program. The data for this paper are available upon request.

References

Afonso, J. C., and D. L. Schutt (2012), The effects of polybaric partial melting on density and seismic velocities of mantle restites, *Lithos*, *134–135*, 289–303.

Afonso, J. C., M. Fernandez, G. Ranalli, W. L. Griffin, and J. A. D. Connolly (2008), Integrated geophysical-petrological modeling of the lithosphere and sublithospheric upper mantle: Methodology and applications, *Geochem. Geophys. Geosyst.*, *9*, Q05008, doi:10.1029/2007GC001834.

Artemieva, I. M. (2006), Global 1° × 1° thermal model TC1 for the continental lithosphere: Implications for lithosphere secular evolution, *Tectonophysics*, *416*, 245–277.

Aulbach, S. (2012), Craton nucleation and formation of thick lithospheric roots, *Lithos*, *149*, 16–30.

Aulbach, S., W. L. Griffin, N. J. Pearson, S. Y. O'Reilly, and B. J. Doyle (2007), Lithosphere formation in the central Slave Craton (Canada): Plume subcretion or lithosphere accretion?, *Contrib. Mineral. Petrol.*, *154*, 409–427.

Becker, T. W., C. Faccenna, E. D. Humphreys, A. R. Lowry, and M. S. Miller (2014), Static and dynamic support of western United States topography, *Earth Planet. Sci. Lett.*, *631*, 65–86.

Bedle, H., and S. van der Lee (2009), *S* velocity variations beneath North America, *J. Geophys. Res.*, *114*, B07308, doi:10.1029/2008JB005949.

Bird, P. (1988), Formation of the Rocky Mountains, western United States: A continuum computer model, *Science*, *239*, 1501–1507, doi:10.1126/science.239.4847.1501.

Boyd, F. R. (1989), Compositional distinction between oceanic and cratonic lithosphere, *Earth Planet. Sci. Lett.*, *96*, 15–26.
Boyd, F. R., N. P. Pokhilenko, D. G. Pearson, S. A. Mertzman, N. V. Sobolev and L. W. Finger (1997), Composition of the Siberian cratonic mantle: Evidence from Udachnaya peridotite xenoliths, *Contrib. Mineral. Petrol.*, *128*, 228–246.
Cammarano, F., S. Goes, P. Vacher, and D. Giardini (2003), Inferring upper-mantle temperatures from seismic velocities, *Phys. Earth Planet. Inter.*, *138*, 197–222, doi:10.1016/S00319201(03)00156-0.
Carlson, R. W., I. J. Irving, D. J. Schulze, and B. C. Hearn (2004), Timing of Precambrian melt depletion and Phanerozoic refertilization events in the lithospheric mantle of the Wyoming Craton and adjacent Central Plains Orogen, *Lithos*, *77*, 453–472.
Deschamps, F., J. Trampert, and R. Snieder (2002), Anomalies of temperature and iron in the uppermost mantle inferred from gravity data and tomographic models, *Phys. Earth Planet. Inter.*, *129*, 245–264.
Dickinson, W. R. (2004), Evolution of the North American Cordillera, *Annu. Rev. Earth Planet. Sci.*, *32*, 13–45, doi:10.1146/ann.rev.earth.32.101802.120257.
Gaul, O. F., W. L. Griffin, S. Y. O'Reilly, and N. J. Pearson (2000), Mapping olivine composition in the lithospheric mantle, *Earth Planet. Sci. Lett.*, *182*, 223–235.
Godey, S., F. Deschamps, J. Trampert, and R. Snieder (2004), Thermal and compositional anomalies beneath the North American continent, *J. Geophys. Res.*, *109*, B01308, doi:10.1029/2002JB002263.
Goes, S., R. Govers, and P. Vacher (2000), Shallow upper mantle temperatures under Europe from P and S wave tomography, *J. Geophys. Res.*, *105*, 11,153–11,169.
Griffin, W. L., B. J. Doyle, C. G. Ryan, N. J. Pearson, S. Y. O'Reilly, R. M. Davies, K. Kivi, E. van Achterbergh, and L. M. Natapov (1999), Layered mantle lithosphere in the Lac de Gras area, Slave Craton: composition, structure and origin, *J. Petrol.*, *40*, 705–727.
Griffin, W. L., S. Y. O'Reilly, N. Abe, S. Aulback, R. M. Davies, N. J. Pearson, B. J. Doyle, and K. Kivi (2003), The origin and evolution of Archean lithospheric mantle, *Precambrian Res.*, *127*, 19–41.
Griffin, W. L., S. Y. O'Reilly, B. J. Doyle, N. J. Pearson, H. Coopersmith, K. Kivi, V. Malkovets, and N. Pokhilenk (2004), Lithosphere mapping beneath the North American plate, *Lithos*, *77*, 873–922.
Griffin, W. L., S. Y. O'Reilly, J. C. Afonso, and G. C. Begg (2009), The composition and evolution of lithospheric mantle: A re-evaluation and its tectonic implications, *J. Petrol.*, *50*(7), 1185–1204, doi:10.1093/petrology/egn033.
Hasterok, D., and D. S. Chapman (2011), Heat production and geotherms for the continental lithosphere, *Earth Planet. Sci. Lett.*, *307*, 59–70.
Hawkesworth, C. J., R. N. W. Kempton, R. M. Ellam, and P. W. van Calsteren (1990), Continental mantle lithosphere, and shallow level enrichment process in the Earth's mantle, *Earth Planet. Sci. Lett.*, *96*, 256–268.
Herzberg, C. T. (1999), Phase equilibrium constraints on the formation of cratonic mantle, in *Mantle Petrology: Field Observations and High-Pressure Experimentation, Spec Publ.*, edited by Y. Fei, C. M. Bertka, and B. O. Mysen, pp. 241–257, Geochem. Soc., Washington, D. C.
Hildebrand, R. S. (2009), Did westward subduction cause Cretaceous-Tertiary orogeny in the North American cordillera?, *Spec. Pap. Geol. Soc. Am.*, *457*, 1–71.
Hyndman, R. D., and C. A. Currie (2011), Why is the North America Cordillera high? Hot backarcs, thermal isostasy, and mountain belts, *Geology*, *39*, 783–786.
Jackson, I., J. D. Fitz Gerald, U. H. Faul, and B. H. Tan (2002), Grain-size-sensitive seismic wave attenuation in polycrystalline olivine, *J. Geophys. Res.*, *107*(B12), 2360, doi:10.1029/2001JB001225.
Jordan, T. H. (1979), Mineralogies, densities and seismic velocities of garnet lherzolites and their geophysical implications, in *The Mantle Sample: Inclusions in Kimberlites and Other Volcanics*, edited by F. R. Boyd and H. O. A. Meyer, pp. 1–14, AGU, Washington, D. C.
Jordan, T. H. (1988), Structure and formation of the continental tectosphere, *J. Petrol.*, *1988*, 11–37.
Kaban, M. K., M. Tesauro, W. D. Mooney, and S. A. P. L. Cloetingh (2014), Density, temperature, and composition of the North American lithosphere—New insights from a joint analysis of seismic, gravity, and mineral physics data: 1. Density structure of the crust and upper mantle, *Geophys. Geochem. Geosyst.*, *15*, 4781–4807, doi:10.1002/2014GC005483.
Karato, S., and H. Jung (1998), Water partial melting and the origin of the seismic low velocity and high attenuation zone in the upper mantle, *Earth Planet. Sci. Lett.*, *157*, 193–207.
Kelemen, P. B, S. R. Hart, and S. Bernstein (1998), Silica enrichment in the continental upper mantle via melt/rock reaction, *Earth Planet. Sci. Lett.*, *164*, 387–406.
Khan, A., A. Zunino, and F. Deschamps (2011), The thermo-chemical and physical structure beneath the North American continent from Bayesian inversion of surface-wave phase velocities, *J. Geophys. Res*, *116*, B09304, doi:10.1029/2011JB008380.
Khan, A., A. Zunino, and F. Deschamps (2013), Upper mantle compositional variations and discontinuity topography imaged beneath Australia from Bayesian inversion of surface-wave phase velocities and thermochemical modeling, *J. Geophys. Res.*, *118*, 5285–5306, doi:10.1002/jgrb.50304.
Klemme, S. (2004), The influence of Cr on the garnet-spinel transition in the Earth's mantle: Experiments in the system MgO-Cr_2O_3−5iO_2 and thermodynamic modelling, *Lithos*, *77*, 639–646.
Kopylova, M. G., J. Lo, and N. I. Christensen (2004), Petrological constraints on seismic properties of the Slave upper mantle (Northern Canada), *Lithos*, *77*, 493–510.
Kurtz, R. D., and G. D. Garland (1976), Magnetotelluric measurements in Eastern Canada, *Geophys. J. R. Astron. Soc.*, *45*, 321–347.
Lee, C.-T. (2003), Compositional variation of density and seismic velocities in natural peridotites at STP conditions: Implications for seismic imaging of compositional heterogeneities in the upper mantle, *J. Geophys. Res.*, *108*(B9), 2441, doi:10.1029/2003JB002413.
Lee, C.-T. A., and E. Chin (2014), Calculating melting temperatures and pressures of peridotite protoliths: Implications for the origin of cratonic mantle, *Earth Planet. Sci., Lett.*, *403*, 273–286.
Lee, C.-T. A., P. Luffi, and E. J. Chin (2011), Building and destroying continental mantle, *Annu. Rev. Earth Planet. Sci.*, *39*, 59–90.
MacKenzie, J. M., and D. Canil (1999), Composition and thermal evolution of cratonic mantle beneath the central Archean Slave Province, NWT, Canada, *Contrib. Mineral. Petrol.*, *134*, 313–324.
Matsukage, K. N., Y. Nishihara, and S.-I. Karato (2005), Seismological signature of chemical differentiation of Earth's upper mantle, *J. Geophys. Res.*, *110*, B12305, doi:10.1029/2004JB003504.
McDonough,W. F., and S.-S. Sun (1995), The composition of the Earth, *Chem. Geol.*, *120*, 223–253.
Menzies, A., K. Westerlund, H. Grutter, J. Gurney, J. Carlson, A. Fung, and T. Nowicki (2004), Peridotitic mantle xenoliths from kimberlites on the Ekati Diamond Mine property, NWT, Canada: Major element compositions and implications for the lithosphere beneath the central Slave craton, *Lithos*, *77*, 395–412.
Mooney, W. D., and M. K. Kaban (2010), The North American upper mantle: Density, composition, and evolution, *J. Geophys. Res.*, *115*, B12424, doi:10.1029/2010JB000866.

NOAA (2010). [Available at http: //www.ngdc.noaa.gov/mgg/sedthick/sedthick.html.]
Nolet, G., and A. Zielhuis (1994), Low S velocities under the Tornquist-Teisseyre zone: Evidence from water injection into the transition zone by subduction, *J. Geophys. Res.*, *99*, 15,813–15,820.
O'Hara, M. J., M. J. Saunders, and E. P. L. Mercy (1975), Garnet-peridotite, primary ultrabasic magma and eclogite; interpretation of upper mantle processes in kimberlite, *Phys. Chem. Earth*, *9*, 571–604.
Pearson, D. G., and N. Witting (2008), Formation of Archean continental lithosphere and its diamonds: The root of the problem, *J. Geol. Soc.*, *165*, 895–914.
Pearson, D. G., D. Canil, and S. B. Shirey (2003), Mantle samples included in volcanic rocks: Xenoliths and diamonds, in *Treatise on Geochemistry: The Mantle and Core*, vol. 2, edited by H. D. Holland and K. K. Turekian, pp. 171–275, Elsevier, N. Y.
Pollack, H. N., and D. S. Chapman (1977), On the regional variation of heat flow, geotherms, and lithospheric thickness, *Tectonophysics*, *38*, 279–296.
Poudjom Djomani, Y. H., S. O'Reilly, W. L. Griffin, and P. Morgan (2001), The density structure of subcontinental lithosphere through time, *Earth Planet. Sci. Lett.*, *184*, 605–621.
Ritsema, J., A., Deuss, H. J. van Heijst, and J. H. Woodhouse (2011), S40RTS: A degree-40 shear-velocity model for the mantle from new Rayleigh wave dispersion, teleseismic traveltime and normal-mode splitting function measurements, *Geophys. J. Int.*, *184*(3), 1223–1236.
Schaeffer, A. J., and S. Lebedev (2013), Global shear-speed structure of the upper mantle and transition zone, *Geophys. J. Int.*, *194*(1), 417–449.
Schulze, D. J. (1989), Constraints on the abundance of eclogite in the upper mantle, *J. Geophys. Res.*, *94*, 4205–4212.
Schutt, D. L., and C. E. Lesher (2010), Compositional trends among Kaapvaal Craton garnet peridotite xenoliths and their effects on seismic velocity and density, *Earth Planet. Sci. Lett.*, *300*, 367–373.
Simmons, M., A. M. Forte, and S. P. Grand (2009), Joint seismic, geodynamic and mineral physical constraints on three-dimensional mantle heterogeneity: Implications for the relative importance of thermal versus compositional heterogeneity, *Geophys. J. Int.*, *177*, 1284–1304.
Stixrude, L., and C. Lithgow-Bertelloni(2005), Thermodynamics of mantle minerals—I. Physical properties, *Geophys. J. Int.*, *162*, 610–632.
Streckeisen, A. (1976), To each plutonic rock its proper name, *Earth Sci. Rev.*, *12*, 1–33.
Tesauro, M., M. K. Kaban, W. D. Mooney, and S. A. P. L. Cloetingh (2014), NACr14: A 3D model for the crustal structure of the North American Continent, *Tectonophysics*, *631*, 65–86.
Thomas, W. A. (1989), The Appalachian-Ouachita orogen beneath the Gulf Coastal Plain between the outcrops in the Appalachian and Ouachita Mountains, in *The Appalachian-Ouachita Orogen in the United States, Geology of North America*, vol. F-2, edited by R. D. Hatcher Jr., W. A. Thomas and G. W. Viele, pp. 537–553, Geol. Soc. of Am., Boulder, Colo.
van der Lee, S., K. Regenauer-Lieb and D. A. Yuen (2008), The role of water in connecting past and future episodes of subduction, *Earth Planet. Sci. Lett.*, *273*, 15–27.
Walter, M. J. (1998), Melting of garnet peridotite and the origin of komatiite and depleted lithosphere, *J. Petrol.*, *1*, 29–60.
Walter, M. J. (2003), *Melt extraction and compositional variability in mantle lithosphere*, Treatise on Geochemistry, vol. 2, The Mantle and Core, edited by H. D. Holland and K. K. Turekian, pp. 363–394, Elsevier, N. Y.
Yuan, H., and B. Romanowicz (2010), Lithospheric layering in the North American craton, *Nature*, *466*, 1063–1068, doi:10.1038/nature09332.